Role of Mesodermal FGF8 and FGF10 Overlaps in the Development of the Arterial Pole of the Heart and Pharyngeal Arch Arteries

Yusuke Watanabe, Sachiko Miyagawa-Tomita, Stéphane D. Vincent, Robert G. Kelly, Anne M. Moon, Margaret E. Buckingham

Rationale: **The genes encoding fibroblast growth factor (FGF) 8 and 10 are expressed in the anterior part of the second heart field that constitutes a population of cardiac progenitor cells contributing to the arterial pole of the heart. Previous studies of hypomorphic and conditional *Fgf8* mutants show disrupted outflow tract (OFT) and right ventricle (RV) development, whereas *Fgf10* mutants do not have detectable OFT defects.**

Objectives: **Our aim was to investigate functional overlap between *Fgf8* and *Fgf10* during formation of the arterial pole.**

Methods and Results: **We generated mesodermal *Fgf8; Fgf10* compound mutants with *MesP1Cre*. The OFT/RV morphology in these mutants was affected with variable penetrance; however, the incidence of embryos with severely affected OFT/RV morphology was significantly increased in response to decreasing *Fgf8* and *Fgf10* gene dosage. *Fgf8* expression in the pharyngeal arch ectoderm is important for development of the pharyngeal arch arteries and their derivatives. We now show that *Fgf8* deletion in the mesoderm alone leads to pharyngeal arch artery phenotypes and that these vascular phenotypes are exacerbated by loss of *Fgf10* function in the mesodermal core of the arches.**

Conclusions: **These results show functional overlap of FGF8 and FGF10 signaling from second heart field mesoderm during development of the OFT/RV, and from pharyngeal arch mesoderm during pharyngeal arch artery formation, highlighting the sensitivity of these key aspects of cardiovascular development to FGF dosage. (*Circ Res.* 2010;106:495-503.)**

Key Words: second heart field ■ arterial pole defects ■ pharyngeal arch artery defects

Malformations of the arterial pole of the heart account for more than 30% of human congenital heart defects.[1] Remodeling of the outflow tract (OFT) plays a critical role in the maturation of the arterial pole. As the heart matures, cushion tissue is formed in the OFT, as a result of an epithelial–mesenchymal transformation.[2] Rotation and shortening of the OFT are accompanied by fusion of the cushions to form a septum that divides the OFT into the aorta and pulmonary trunk. Subsequent morphogenetic events result in alignment of the aorta with the left ventricle and the pulmonary trunk with the right ventricle (RV).[3] The OFT is derived from the anterior part of the second heart field (SHF), which in the mouse embryo, also contributes to the RV and ventricular septum.[4–6] This field of splanchnic mesoderm initially lies medial to the cardiac crescent and then dorsally and anteriorly to the heart tube. In addition to myocardium, the SHF contributes smooth muscle to the base of the great arteries.[6,7] A second source of cells, namely cardiac neural crest (CNC), migrates from the neuroectoderm of the dorsal neural tube into the OFT and contributes to cushion formation and correct septation and alignment of the aortic and pulmonary outflows.[8–10] CNC also interacts with the mesodermal cells of the SHF.[11] When CNC is ablated in the chick embryo, OFT elongation and looping of the cardiac tube is perturbed, leading to persistent truncus arteriosus and misalignment of the great arteries relative to the ventricles.[10] Many signaling pathways in the SHF, CNC, and pharyngeal region control development of the arterial pole of the heart by affecting specification, proliferation, survival and differentiation of progenitor cells.[12]

SHF mesoderm also plays a role in the formation of the blood vessels that channel blood from the aorta and pulmonary trunk to the body and lungs. These arteries form within the third, fourth, and sixth pharyngeal arches, which are bilateral embryonic structures, consisting of surface ectoderm, inner endoderm, and a mesodermal core expressing SHF markers, that becomes surrounded by CNC. The endothelium of the pharyngeal arch

Original received May 26, 2009; revision received December 8, 2009; accepted December 10, 2009.

From the Department of Developmental Biology (Y.W., S.D.V., M.E.B.), Centre National de la Recherche Scientifique, Unité de Recherche Associée 2578, Institut Pasteur, Paris, France; Department of Pediatric Cardiology (S.M.-T.), Tokyo Women's Medical University, Tokyo, Japan; Developmental Biology Institute of Marseille-Luminy (R.G.K.), Unité Mixte de Recherche 6216 Université de la Méditerranée, Campus de Luminy, Marseille, France; and Departments of Pediatrics, Neurobiology, and Anatomy and Human Genetics (A.M.M.), University of Utah, Salt Lake City. Present address for Y.W.: Department of Developmental Neurobiology, Institute of Development, Aging and Cancer, Tohoku University, Sendai, Miyagi, Japan.

Correspondence to Margaret Buckingham, DPhil, Department of Developmental Biology, URA CNRS 2578, Institut Pasteur, 25 rue du Dr. Roux 75015 Paris, France. E-mail margaret.buckingham@pasteur.fr

Circulation Research is available at http://circres.ahajournals.org DOI: 10.1161/CIRCRESAHA.109.201665

Non-standard Abbreviations and Acronyms	
CNC	cardiac neural crest
DORV	double outlet right ventricle
E	embryonic day
FGF	fibroblast growth factor
FGFR	fibroblast growth factor receptor
OFT	outflow tract
PAA	pharyngeal arch artery
RV	right ventricle
SHF	second heart field
VSD	ventricular septal defect

arteries (PAAs) is formed from the mesodermal core of the arches, whereas the vascular smooth muscle is predominantly CNC-derived.[8,13,14] The PAAs form progressively following the anterior/posterior gradient of pharyngeal arch development, and from embryonic day (E)10.5 in the mouse embryo, remodeling leads to the mature PAA system. Many different cellular and genetic perturbations disrupt formation and /or remodeling of the PAAs.[10]

Fgf10 was identified as a gene expressed in cells that contribute to the OFT and RV in the mouse embryo, leading to the concept of the SHF.[15] However *Fgf10*-null mutants have no evident SHF or PAA defects.[16] *Fgf8* expression overlaps with that of *Fgf10* in the SHF from the cardiac crescent stage.[15] Their expression is restricted to the anterior part of the SHF and is regulated by retinoic acid signaling on the anterior-posterior axis.[17] *Fgf10* transcription extends from the anterior SHF into the mesodermal core of the pharyngeal arches, where *Fgf8* transcripts are difficult to detect. However, $Fgf8^{LacZ/+}$, $Fgf8^{GFP/+}$, and *Fgf8* enhancer-*LacZ* transgenic mice show LacZ or green fluorescent protein (GFP) expression in the anterior SHF and the mesodermal core of the arches, implying that *Fgf8* is transcribed there.[18–20] Unlike *Fgf10*, *Fgf8* is also expressed in pharyngeal endoderm and ectoderm, where its expression is maintained, at least until E9.5.[21] *Fgf8* mutants die at gastrulation[22]; however, *Fgf8* hypomorphs survive to birth with variable OFT defects including persistent truncus arteriosus, transposition of the great arteries, and pharyngeal arch-related phenotypes. The fourth PAA is most severely affected resulting in interrupted or right aortic arch.[23,24] Apoptosis of CNC was noted in these hypomorphs, suggesting fibroblast growth factor (FGF)8 signaling defects in surrounding tissues that directly or indirectly affect CNC, because *Fgf8* is not expressed in these cells. Subsequently, conditional mutagenesis of *Fgf8* with a battery of Cre recombinases, directed to pharyngeal ectoderm, pharyngeal endoderm, and SHF/pharyngeal arch mesoderm, has allowed tissue-specific phenotypes to be determined.[13,19,20,25] Deletion of *Fgf8* in the pharyngeal ectoderm leads to CNC apoptosis, affecting PAA development.[25] The role of mesodermal FGF8 in PAA development has not been reported. Mesodermal and endodermal FGF8 are critical for OFT development, affecting the proliferation, survival, and transcriptional activity of SHF cells and their derivatives, in addition to the function of the CNC. Deletion of *Fgf8* in early cardiogenic mesoderm with *MesP1Cre* causes initial OFT/RV hypoplasia and OFT alignment defects in survivors at incomplete penetrance.[19] This implies that FGF10 may compensate for loss of FGF8 in the precardiac mesoderm.

In this study, we generated compound *Fgf8* and *Fgf10* mutants in the cardiac and pharyngeal mesoderm, using *MesP1Cre*. We show that PAA development is perturbed by mesodermal *Fgf8* deletion. The incidence and severity of PAA and of OFT defects increased with decreasing *Fgf8* and *Fgf10* gene dosage, resulting in severe defects in double *Fgf8*;*Fgf10* homozygous conditional mutants. These results reveal functional overlap of mesodermal FGF8 and FGF10 during SHF/OFT and PAA development, uncovering for the first time a role for FGF10 in the formation of the arterial pole of the heart. They also illustrate the sensitivity of these processes to incremental reductions in the level of FGF.

Methods

Mouse Lines

Mouse care and procedures were in accordance with institutional and national guidelines. The *Fgf8*-conditional mutant, *Fgf10* mutant, and *MesP1Cre* alleles are as previously described.[19,26,27] The $MesP1^{Cre/+}$ line was bred onto an $Fgf10^{+/-}$ background and then onto $Fgf8^{flox/+}$, which was crossed with an $Fgf8^{flox/flox}$;$Fgf10^{+/-}$ line to obtain compound mutants. *Fgf8* and *Fgf10* genotyping by PCR was performed using the following primers: P1, P2, and 5′-GAGCTTGCTGGGGGAAACTTCCTGACTAGG-3′ for $Fgf10^{26}$; and 5′-TGCCTAAGGGGAGAAGGCTGG-3′, 5′-AAATTTAAGCTGTGTAGATTCCATAG-3′, and 5′-GATTTCAGGAGAACAGACCAGAG-3′ primers for *Fgf8*. Numbers of embryos obtained at different stages are summarized in Online Table I (available in the Online Data Supplement at http://circres.ahajournals.org). Total numbers of embryos examined for each genotype at E10.5 and E15.5 to 18.5 are given in Tables 1 and 2, respectively.

Scoring OFT and RV Morphology

Right-sided views of the OFT and RV in embryos at E9.5 were scored according to four parameters, OFT length, the angle between the proximal and distal regions of the OFT, the size of the RV, and the extent of looping estimated by the angle of the OFT across the ventral body of the embryo. Scoring was performed by two independent observers blinded to genotype. There was remarkably little interobserver variability in the scores of individual embryos of all genotypes (not shown). Embryos were classified as normal, mild, moderate, and severe depending on the score (2 points for each parameter, with a maximum of 8 points: <2 points, severe; <4 points, moderate; <6 points, mild; ≥ 6, normal).

Histological Analysis and Ink Injection

Longitudinal sections (10 μm) were made in the OFT and pharyngeal arch region after paraffin embedding of E10.5 embryos. To visualize PAA formation, India ink was injected into the left ventricle or umbilical vein of E10.5 embryos using drawn glass pipettes.

Quantitative Real-Time PCR

The third to sixth pharyngeal arch region was dissected from embryos at 24 to 26 somite stages and stored in RNAlater (Qiagen) at -20°C until use. Total RNA was isolated from a pool of six samples for each genotype using RNeasy Mini Kit (Qiagen). The first strand cDNA was synthesized using SuperScript II Reverse Transcriptase (Invitrogen). Quantitative PCR was performed with Power SYBR Green PCR Master Mix (Applied Biosystems) with the StepOnePlus Real-Time PCR system (Applied Biosystems). Reverse transcription and quantitative PCR were repeated 3 times, and *Gapdh* was used to normalize gene expression. Primer sequences were 5′-TGAAAGGCGGATACTTG-

Table 1. Incidence of Abnormal PAAs in *Fgf8;Fgf10* Compound Mutants With *MesP1Cre* at E10.5

		Second PAA			Third PAA			Fourth PAA			Sixth PAA				
			Presence			Absence			Absence			Absence		PAA Total	
Fgf8;Fgf10 Genotype	No. of Embryos Examined	Normal	Uni	Bi	Normal	Uni	Bi	Normal	Uni	Bi	Normal	Uni	Bi	Normal	Abnormal
flox/+;+/+	10	10	0	0	10	0	0	10	0	0	8	0	2	8	2
flox/+;+/−	14	14	0	0	14	0	0	13	1	0	14	0	0	13	1
flox/+;−/−	3	3	0	0	3	0	0	3	0	0	3	0	0	3	0
flox/flox;+/+	16	15	0	1	11	4	1	12	4	0	15	0	1	8	8
flox/flox;+/−	13	11	2	0	8	5	0	8	5	0	13	0	0	6	7
flox/flox;−/−	7	4	1	2	4	2	1	1	4	2	7	0	0	0	7

PAAs examined after ink injection as shown in Figure 3. Unilateral (Uni) or bilateral (Bi) defects were scored as abnormal in all cases. χ^2 test was applied in comparisons of the following examples in the table. Second PAA: $^*P<0.05$, $Fgf8^{flox/flox}$ vs $Fgf8^{flox/flox};Fgf10^{-/-}$; fourth PAA: $^{**}P<0.01$, $Fgf8^{flox/flox}$ vs $Fgf8^{flox/flox};Fgf10^{-/-}$; $^*P<0.05$, $Fgf8^{flox/flox};Fgf10^{+/-}$ vs $Fgf8^{flox/flox};Fgf10^{-/-}$; PAA total: $^*P<0.05$, $Fgf8^{flox/flox}$ vs $Fgf8^{flox/flox};Fgf10^{-/-}$ and $Fgf8^{flox/flox};Fgf10^{+/-}$ vs $Fgf8^{flox/flox};Fgf10^{-/-}$.

GAC-3′ and 5′-TGTCCGGTACCTGAGCTTCT-3′ for *Pea3*; 5′-GGACACAGATCTGGCTCACGA-3′ and 5′-CGTGGCTACAGGACGACAAC-3′ for *Erm*; *Isl1* primers were as designed by Liao et al.[28]

Results

Fgf10 expression is observed in the anterior SHF and pharyngeal mesoderm, whereas *Fgf8* is expressed in pharyngeal endoderm and ectoderm in addition to these mesodermal tissues. To generate compound mutants for *Fgf8* and *Fgf10* in this mesoderm, we deleted the *Fgf8* conditional allele ($Fgf8^{flox}$) with $MesP1^{Cre/+}$. *Fgf10*-null homozygotes are not viable after birth, and we therefore used the *Fgf10* heterozygotes ($Fgf10^{+/-}$) for crosses (see Online Table I, $Fgf8^{flox/+};Fgf10^{+/-};MesP1^{Cre/+}\times Fgf8^{flox/flox};Fgf10^{+/-}$). In the following text, $MesP1^{Cre/+}$ is included in all genotypes.

OFT and RV Morphology Is Affected by Reducing *Fgf8* and *Fgf10* Dosage

In *Fgf8;Fgf10* double heterozygous ($Fgf8^{flox/+};Fgf10^{+/-}$) (Figure 1B) and $Fgf8^{flox/+};Fgf10^{-/-}$ embryos (Figure 1C), OFT and RV morphology is normal at E9.5, similar to that of $Fgf8^{flox/+}$ embryos (Figure 1A). $Fgf8^{flox/flox}$ embryos have hypomorphic OFTs and RVs (Figure 1D through 1F), as previously reported with a *MesP1Cre* at E9.5.[19] When *Fgf10* dosage was decreased in addition to *Fgf8* deletion (Figure 1G through 1L), more severe phenotypes were observed, including hypoplasia of the second and third pharyngeal arches (Figure 1I and 1L). This was also illustrated by sections of the OFT at E10.5 showing normal presence of CNC and initiation of epithelial–mesenchymal transition before cushion formation in control *Fgf8;Fgf10* double heterozygotes (Figure 1M). In contrast, CNC invasion and epithelial–mesenchymal transition were notably compromised in *Fgf8;Fgf10* double homozygous mutants (Figure 1O) and already affected in $Fgf8^{flox/flox}$ mutants (Figure 1N).

To confirm and quantify this, we scored OFT and RV morphology on the basis of OFT length, the angle between the proximal and distal regions of the OFT, RV size and extent of looping, by a blind test. Phenotypes were classified as normal, mild, moderate, and severe, depending on the score (Figure 2A). The number of abnormal $Fgf8^{flox/flox}$ embryos was less than in our previous report, probably because in that case the $Fgf8^{flox/-}$ cross was analyzed.[19] The important point, shown in Figure 2A, is that increasingly affected embryos were observed as *Fgf* dosage is reduced. No severe phenotypes were observed with *Fgf8* deletion alone, whereas no normal hearts were observed in *Fgf8;Fgf10* double homozygous mutants. This result shows that FGF10 functions with FGF8 in OFT and RV development. To verify that FGF signaling was attenuated in *Fgf8;Fgf10* double homozygous mutants, we performed quantitative PCR analysis for FGF target genes, *Pea3* and *Erm*, using RNA isolated from the pharyngeal region (including SHF mesoderm, endoderm,

Table 2. Incidence of Abnormal Heart and PAAs in *Fgf8;Fgf10* Compound Mutants With *MesP1Cre* at E15.5 to E18.5

		Heart			Pharyngeal Arch Arteries				
Fgf8;Fgf10 Genotype	No. of Embryos Examined	Normal	TGA/DORV	VSD	Normal	Short or Absent LCC	ARSA	RtAA	Narrow AoA
flox/+;+/+	7	7	0	0	7	0	0	0	0
flox/+;+/−	13	13	0	0	13	0	0	0	0
flox/+;−/−	4	4	0	0	4	0	0	0	0
flox/flox;+/+	11	9	1	2	8	2	1	1	0
flox/flox;+/−	13	8	1	5	9	2	2	1	1
flox/flox;−/−	5	1	1	3	1	2	2	0	1

One or more arterial pole or PAA malformations were scored as abnormal in all cases. χ^2 test was applied in comparisons of the following examples in the table. Heart: $^*P=0.018$, $Fgf8^{flox/flox}$ vs $Fgf8^{flox/flox};Fgf10^{-/-}$; PAAs: $^*P=0.049$, $Fgf8^{flox/flox}$ vs $Fgf8^{flox/flox};Fgf10^{-/-}$. AoA indicates aortic arch; ARSA, aberrant origin of right subclavian artery; RtAA, right aortic arch; TGA, transposition of the great arteries.

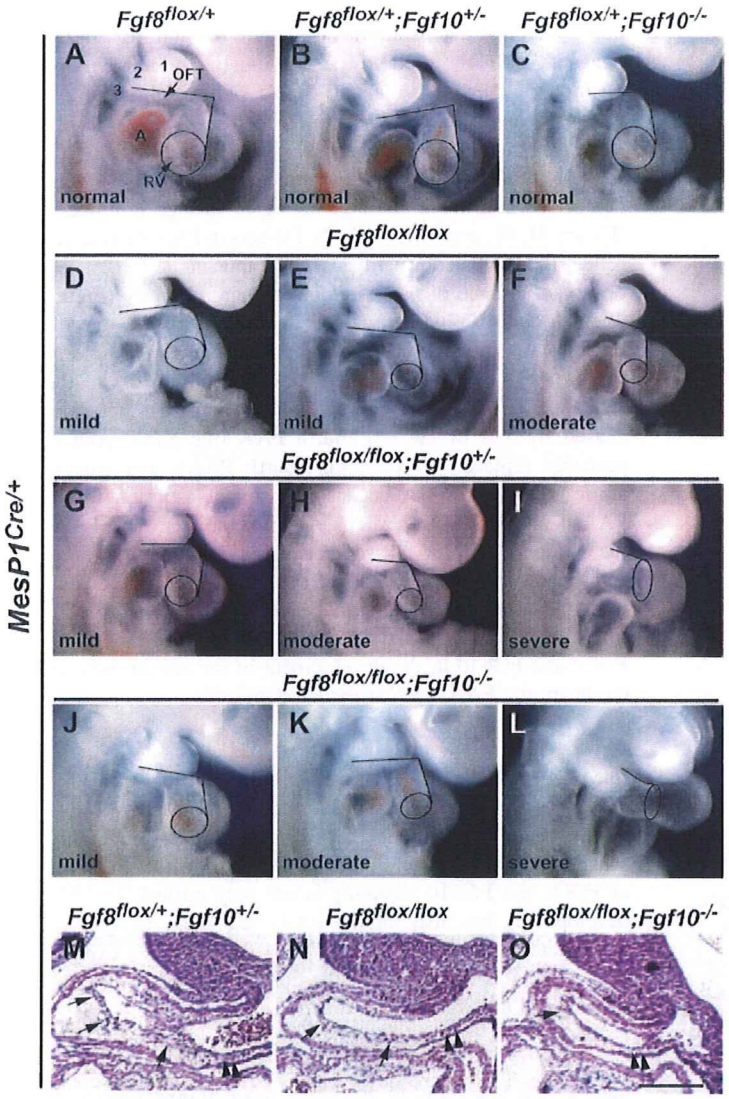

Figure 1. OFT and RV morphology of E9.5 *Fgf8;Fgf10;MesP1Cre* compound mutants. A through L, Right lateral views of embryos are shown, and genotypes are listed above the images. In $Fgf8^{flox/+}$ (A), $Fgf8^{flox/+};Fgf10^{+/-}$ (B), and $Fgf8^{flox/+};Fgf10^{-/-}$ (C) embryos, OFT and RV morphology is normal. In $Fgf8^{flox/flox}$ (D through F), $Fgf8^{flox/flox};Fgf10^{+/-}$ (G through I), and $Fgf8^{flox/flox};Fgf10^{-/-}$ (J through L) embryos, the angle between the proximal and distal regions of the OFT is more obtuse (lines) or, in severe cases, absent, and/or the RV is smaller (circle) when compared with normal hearts (A through C). M through O, Sections of the OFT of E10.5 embryos with the genotypes indicated. CNC has invaded the OFT (arrowheads), and the endothelium is beginning to undergo epithelial–mesenchymal transformation[31] (arrows), where the cushions will form in *Fgf8;Fgf10* double heterozygous control embryos (M). In *Fgf8;Fgf10* mutant embryos, these processes are compromised (N and O) and most notably in the double homozygous mutant, the OFT is smaller and misshapen (O). Pharyngeal arches are numbered in A. Scale bar=200 μm.

and ectoderm) of compound mutant embryos (Figure 2B). We could not detect differences between $Fgf8^{flox/+};Fgf10^{+/-}$ and $Fgf8^{flox/flox};Fgf10^{+/-}$ mutants, suggesting that FGF8 in pharyngeal endoderm and ectoderm, together with FGF10 from 1 allele of *Fgf10* expressed in mesoderm, lead to levels of *Pea3* and *Erm* transcription in the pharyngeal region that obscure the reduction in the mesoderm. However, significant downregulation of the signaling read out from all FGF sources was detected in *Fgf8;Fgf10* double homozygous mutants (Figure 2B). These results demonstrate the effect on FGF signaling readout of removing both alleles of *Fgf10* on an *Fgf8* mesodermal–null background. Transcripts for *Isl1*, a key transcription factor required in the SHF,[29] were also downregulated in the double homozygous mutants (Figure 2B). Apoptosis and proliferation were altered in Isl1-positive SHF cells in the double homozygous mutants (Online Figure I, A through D), as reported for $Fgf8^{flox/-}$ mutants,[19] thus explaining the reduction in *Isl1* transcripts.

Mesodermal FGF8 and FGF10 Regulate Development of the PAAs

PAAs, visualized by ink injection, were examined in *Fgf8;Fgf10* compound mutants at E10.5 (Figure 3). At this stage, normal mouse embryos have third, fourth, and sixth bilateral PAAs (Figure 3A through 3C). PAA development was affected in some $Fgf8^{flox/flox}$ embryos (Figure 3D through 3F and 3M). Ectodermal *Fgf8* ablation causes bilateral fourth PAA hypoplasia or aplasia.[25] With mesodermal deletion of *Fgf8*, we observed not only fourth PAA defects but also effects on the development of the third and sixth PAAs and abnormal maintenance of the second PAA (Figure 3M). $Fgf10^{-/-}$ mutants did not show any PAA defects, as reported previously (data not shown).[30] However, deletion of one allele of *Fgf10* increased the proportion of PAA defects in $Fgf8^{flox/flox}$ embryos (Figure 3G through 3I and 3M), and this incidence was further increased in *Fgf8;Fgf10* double homozygous mutants (Figure 3J through 3M). Apoptosis in CNC was observed at the level of the developing fourth PAA,

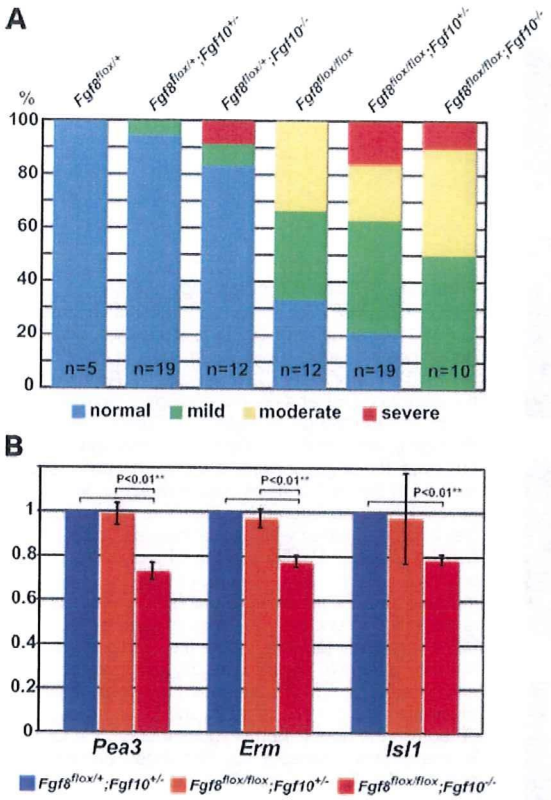

Figure 2. Reduction of FGF dosage affects morphology and gene expression in the OFT and RV. A, Phenotype of OFT and RV morphology of E9.5 *Fgf8;Fgf10;MesP1Cre* compound mutants are divided into normal, mild, moderate, and severe according to OFT length, the angle between the proximal and distal regions of the OFT, RV size, and looping, based on blind tests. Increasingly severe phenotypes (see Figure 1) are observed as *Fgf* gene dosage is reduced. Numbers of embryos (n) are indicated below each column. B, Quantitative PCR analysis of transcripts for FGF signaling effectors, *Pea3* and *Erm*, and for Isl1, normalized to *Gapdh* transcripts, in extracts from the pharyngeal region dissected from 6 embryos, with the genotypes indicated, at 24 to 26 somite stages. Results are shown relative to that for *Fgf8;Fgf10* double heterozygotes. Error bar indicates the SD.

in $Fgf8^{flox/flox};Fgf10^{+/-}$ mutants (Online Figure I, E and F), as reported for *Fgf8* hypomorphic, $Fgf8^{flox/-}$;*AP2aIresCre*, and $Fgf8^{flox/-}$;*Hoxa3Cre* mutants.[23,25] Sections also illustrated the severe PAA defects seen in *Fgf8;Fgf10* double homozygous mutants (Figure 3O), compared to control *Fgf8;Fgf10* double heterozygous embryos (Figure 3N). These results, summarized in Table 1, show that mesodermal FGF8 and FGF10 are critical for PAA development.

Heart and PAA Phenotypes at Later Developmental Stages Are Consistent With Those Observed Earlier

The adult configuration of the heart and great vessels is largely established by E15.5: the ventricles are separated by the ventricular septum; the OFT has given rise to myocardium at the base of the aorta and pulmonary trunk; and the third, fourth, and sixth PAAs have been remodeled into the common carotid and subclavian arteries and contributed to part of the aortic arch and ductus arteriosus (Figure 4A and 4B). In the heart of $Fgf8^{flox/flox}$ embryos, as previously reported,[19] transposition of the great arteries, double outlet right ventricle (DORV), and ventricular septal defects (VSDs) were observed, although in a minority of cases (Figure 4F and 4G; Table 2). In $Fgf8^{flox/flox}$;*Fgf10* compound mutants, these heart defects became more frequent as *Fgf10* dosage is reduced (Figure 4J, 4L, and 4M; Table 2). Defects in PAA derivatives reflect the PAA abnormalities seen in mutants at E10.5. We observed absence of the left common carotid artery (Figure 4E, 4H, and 4K), which was attributable to loss of the left third PAA; aberrant origin of the right subclavian artery (Figure 4F, 4I, and 4K), which is attributable to loss of the right fourth PAA; right aortic arch (Figure 4I), which is caused by loss of the left fourth PAA (the aortic arch is probably replaced by the right fourth PAA); and narrow aortic arch (Figure 4L), because of a hypoplastic left fourth PAA. Consistent with earlier defects of the heart and PAA, the incidence of these later defects in surviving embryos was significantly increased when *Fgf10* gene dosage was reduced, in conjunction with mesodermal deletion of *Fgf8* (Table 2). These results confirm the functional overlap of mesodermal FGF8 and FGF10 in the development of the arterial pole of the heart and PAA, seen at earlier stages.

Discussion

The phenotypic analysis that we present establishes a role for FGF10 as well as FGF8 in the formation of the arterial pole of the heart and demonstrates that this process is highly sensitive to FGF dosage. Furthermore, we show that the level of FGF8 and FGF10 signaling is not only critical for OFT development, but also for the PAAs and their derivatives. Unexpectedly, mesodermal, as well as ectodermal,[25] expression of *Fgf8* is important for the correct formation of these arteries and thus for cardiac function.

Most of the mutant embryos survive to late fetal stages, permitting analysis of the definitive morphology of the arterial pole. This is in contrast to previously reported observations on $Fgf8^{flox/-}$;$MesP1^{Cre/+}$ embryos of which 65% died by E10.5.[19] This difference probably reflects the mesodermal specificity of deletion of the floxed alleles, which in our case ($Fgf8^{flox/flox}$;$MesP1^{Cre/+}$) are entirely responsible for generating the mutant phenotype. At early stages, in *Fgf8* and in *Fgf8;Fgf10* mutants, we observe hypoplasia of both the OFT and RV, which also derives from SHF cells expressing *Fgf8*,[15,20] as well as *Fgf10*.[15] This reflects apoptosis and loss of proliferation of progenitor cells, observed when FGF signaling is abrogated, attributable either to mutation of mesodermal *Fgf8* and *Fgf10* (in this study)[19] or to interference with FGF signal reception in the SHF.[31,32] A reduction in SHF cells is also indicated by a decrease in *Isl1* expression, reported for the more severe $Fgf8^{flox/-}$;*MesP1Cre* phenotype[19] and notable in $Fgf8^{flox/flox}$;$Fgf10^{-/-}$ double mutants. As the OFT matures, leading to epithelial–mesenchymal transition, cushion formation is initiated and CNC migrates into the OFT. These processes are affected when FGF signaling in mesoderm is abrogated,[31,32] and the phenotypes again are striking in the $Fgf8^{flox/flox}$;$Fgf10^{-/-}$ double mutants. The effects of FGF signaling from the SHF on CNC are indirect, because the arterial pole of the heart develops normally when FGF signaling

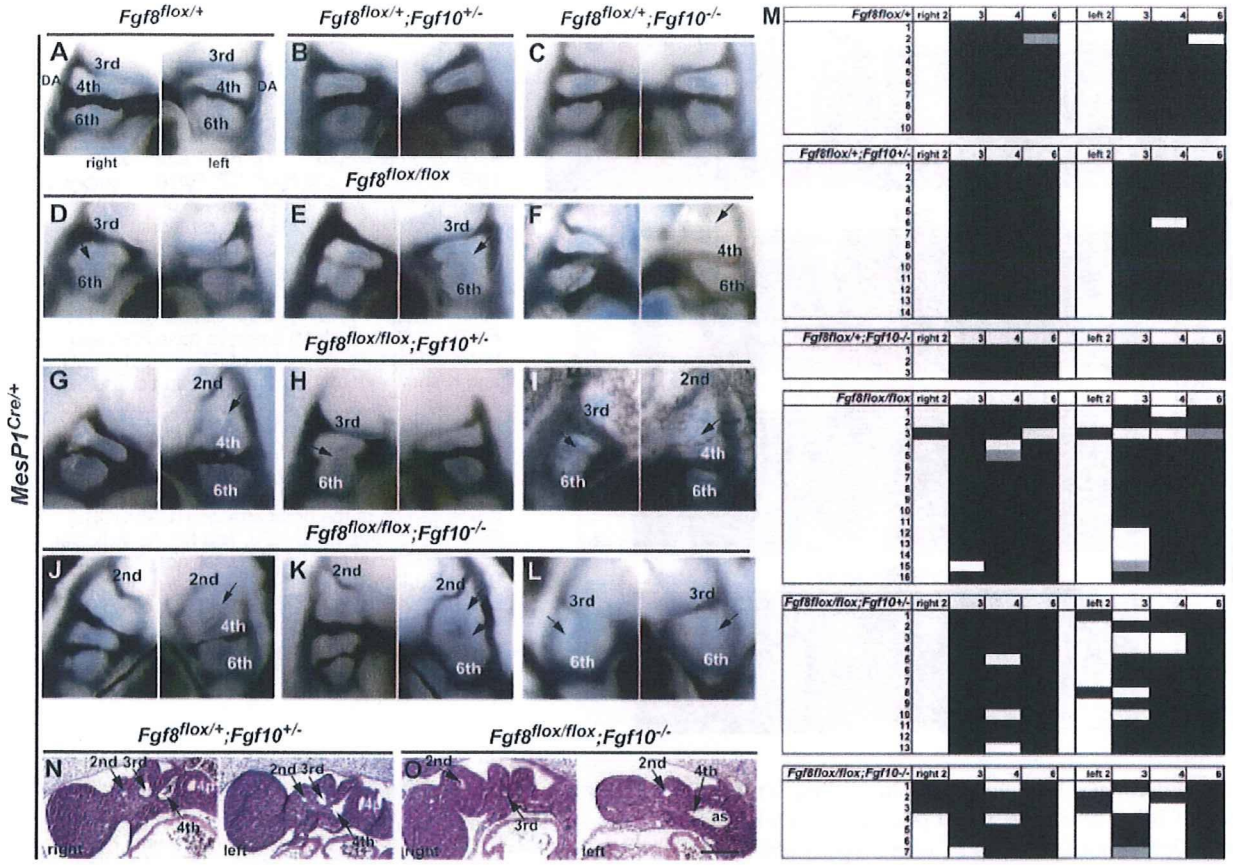

Figure 3. PAAs in *Fgf8;Fgf10;MesP1Cre* compound mutants. A through L, PAAs are visualized by ink injection at E10.5. Genotypes are listed above the images. At E10.5, third, fourth, and sixth PAAs are observed in the arches on both sides of the embryo. $Fgf8^{flox/+}$, $Fgf8^{flox/+}$;$Fgf10^{+/-}$, and $Fgf8^{flox/+}$;$Fgf10^{-/-}$ embryos have normal PAA patterns (A through C), whereas $Fgf8^{flox/flox}$, $Fgf8^{flox/flox}$;$Fgf10^{+/-}$ and $Fgf8^{flox/flox}$;$Fgf10^{-/-}$ embryos have various defects (arrows in D through L), including missing third, fourth, and sixth PAAs, and retention of the second PAA. M, Summary of ink injection results for each embryo examined. Black columns represent PAAs labeled by the ink; white columns, PAAs where ink labeling was negative; gray columns, PAAs that were weakly labeled. N and O, Sections of embryos at E10.0 in the region of the pharyngeal arches, with the genotypes indicated. In control *Fgf8;Fgf10* double heterozygous embryos, the second, third, and fourth arches are evident (N, arrows). The fourth pharyngeal pouch (4p) is also visible. In the *Fgf8;Fgf10* double homozygous mutant sections shown, the fourth arch is present but the PAA is not detectable on the right-hand side. On the left side, the third PAA is missing (O). as indicates aortic sac; DA, dorsal aorta. Scale bar=200 μm.

in CNC is diminished.[31,32] We propose that the Bmp/TGFβ pathway mediates the action of mesodermal FGF signaling on CNC, because components of this pathway are downregulated in *Fgf8* mutants.[31] This would also have effects on the Nkx2.5 transcriptional network in the SHF.[33] Further identification of targets of Pea3/Erm, transcriptional effectors of FGF signaling, should provide more insight into the FGF regulatory network. Failure of CNC migration into the OFT probably results from abnormal cell death in the pharyngeal arches.[20,23–25] Upregulation of FGF signaling, observed with CNC ablation[34] or in *Tbx3* mutants,[35] also disrupts OFT development, demonstrating a critical requirement for precise levels of FGF signaling during arterial pole formation. Because CNC contributes the smooth muscle of the nascent PAAs and their mature derivatives, CNC death in *Fgf8*; *Fgf10;MesP1Cre* compound mutants contributes to defects in the stabilization and remodeling of these arteries. In $Fgf8^{flox/-}$; *AP2αIresCre* mutants where *Fgf8* was deleted in pharyngeal ectoderm, major defects in the fourth PAA were documented, with minor effects on third and sixth PAAs.[25] *Fgf8* deletion in the mesodermal core of the arches causes similar effects on third, fourth and sixth PAAs. The increase in PAA defects in $Fgf8^{flox/flox}$; $Fgf10^{-/-}$ double mutants reveals an unsuspected role for FGF10 in PAA development. We also observe some cases of second PAA persistence at E10.5, probably reflecting a developmental delay. Mesodermal FGF signaling is clearly also necessary and the timing of this requirement may precede the appearance of CNC. *MesP1Cre* is activated at about E6.5, well before somites begin to form, whereas the *Mef2c* regulatory element that drives *Mef2cCre* expression in the SHF, including pharyngeal arch mesoderm, is activated later, from 2 to 3 somite stages.[19] Because PAA formation and remodeling are normal in $Fgf8^{flox/-}$; *Mef2cCre* embryos (16/16; A.M.M., unpublished data, 2005) the *MesP1Cre* phenotypes indicate that mesodermal FGF signaling is required at early stages to support PAA development, before CNC arrive in the arches.

Cardiac defects in surviving *Fgf8;Fgf10* mutants, present as alignment defects of the aorta and pulmonary trunk (transposition of the great arteries) together with DORV and

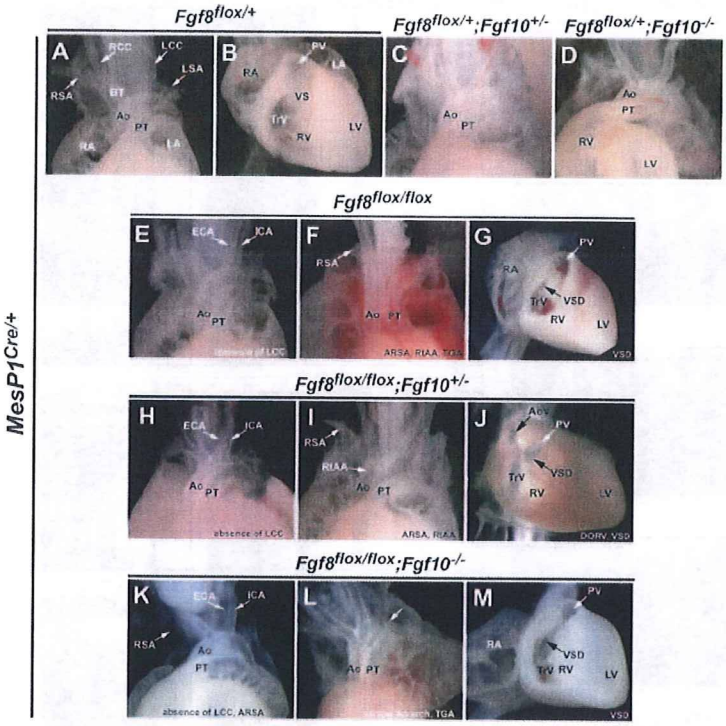

Figure 4. Heart and PAA defects in *Fgf8;Fgf10; MesP1Cre* compound mutants at later stages (E15.5 to E18.5). Genotypes are listed above the images. A through C, Heart and PAAs have normal structures in $Fgf8^{flox/+}$ and $Fgf8^{flox/+};Fgf10^{+/-}$ embryos. In $Fgf8^{flox/+}Fgf10^{-/-}$ and $Fgf8^{flox/flox};Fgf10^{-/-}$ embryos (D and K through M), in the absence of FGF10, the position of the apex of the heart is random, and the pulmonary arteries are absent; other parts of the $Fgf8^{flox/+};Fgf10^{-/-}$ heart and the PAAs are normal (D). E through M, $Fgf8^{flox/flox}$ (E through G), $Fgf8^{flox/flox};Fgf10^{+/-}$ (H through J), and $Fgf8^{flox/flox}; Fgf10^{-/-}$ (K through M) embryos have PAA and heart defects. As examples of PAA defects, E, H, and K show external and internal carotid arteries (ECA and ICA) directly arising from the aortic arch, F, I, and K show an aberrant origin of the right subclavian artery (ARSA), and an abnormal right aortic arch (RtAA) is also observed (I). Heart defects include abnormal alignment of the OFT (transposition of the great arteries [TGA]; DORV) (F, J, and L) and VSDs (G, J, and M). Ao indicates aorta; AoV, aortic valve; BT, brachiocephalic trunk; LA, left atrium; LCC, left common carotid artery; LSA, left subclavian artery; LV, left ventricle; PT, pulmonary trunk; PV, pulmonary valve; RA, right atrium; RCC, right common carotid artery; RSA, right subclavian artery; TrV, tricuspid valve; VS, ventricular septum.

VSDs, reflecting earlier malpositioning of the OFT and affected CNC. These defects also predominate when mesodermal *Fgf8* is mutated (Table 2), whereas persistent truncus arteriosus is seen when *Fgf8* is deleted in both mesoderm and pharyngeal endoderm.[13,19] The defects that we observe later in carotid and subclavian arteries and in the aortic arch reflect earlier defects in PAA development. When *Fgf8* is deleted in pharyngeal ectoderm,[25] the range and frequency of defects is different from those observed with mesodermal deletion of *Fgf8*, or when *Fgf10* is also mutated. In addition to dose dependence, this result reveals the importance of paracrine effects of FGF signaling during PAA development.

Deletion of *Fgf8* and *Fgf10* does not result in total loss of the structures that depend on FGF signaling. This may be because other signaling pathways, such as Bmp/TGFβ, which lies downstream of FGF8,[19] also function independently to promote formation of the arterial pole of the heart and the PAAs. It may also reflect the ability of other FGFs to compensate in the SHF and pharyngeal arches. *Fgf15*, for example, is expressed in pharyngeal mesoderm and *Fgf15* mutants have cardiac defects (DORV, overriding aorta and VSD), suggesting that FGF15 may play a role in the development of the arterial pole of the heart.[36] Loss of *Fgf3*, which is also expressed in pharyngeal endoderm, does not cause heart or PAA phenotypes, but $Fgf3^{-/-};Tbx1^{+/-}$ mutants have an aberrant origin of the right subclavian artery and interrupted aortic arch.[37]

In considering the relative roles of FGF8 and FGF10, the former is more widely produced, by pharyngeal endoderm and pharyngeal ectoderm, as well as by mesoderm in the anterior SHF and in its extension into the core of the pharyngeal arches, whereas FGF10 production is predominantly limited to the mesoderm. Both FGFs bind to FGF receptor (FGFR)2, although FGF10 binds preferentially to the IIIb isoform, whereas FGF8 binds to IIIc and also has affinity for FGFR1, FGFR3IIIc, and FGFR4.[38–40] Mutational analysis of *Fgfr1* and *Fgfr2* suggests that FGFR1 is the dominant receptor in the SHF,[31] although FGFR2 is also active and indeed in a different genetic background may be more important.[32] Mutation of *Fgfr1* and *Fgfr2* in mesoderm compromises OFT development, as does overexpression of Sprouty2, an inhibitor of intracellular FGF signaling.[31] Examination of *Fgfr2-IIIb* mutants shows later cardiac defects,[16] but no striking effects on the early OFT, although RV hypoplasia, overriding aorta, DORV, and VSDs were noted. The question of in vivo FGF/receptor specificity is complex and the only clear conclusion to date is that FGFR1 and FGFR2 are required for FGF8 and FGF10 signaling, playing an essential role in the control of SHF progenitor cell proliferation and downstream signaling cascades[31] during OFT morphogenesis.

The *Tbx1* mutant phenotype, which recapitulates cardiovascular aspects of human DiGeorge syndrome,[41–43] overlaps with that of *Fgf8* hypomorphs.[23,24] *Tbx1* is expressed in the mesoderm of the anterior SHF, including the mesodermal core, endoderm, and ectoderm of the pharyngeal arches,[44,45] like *Fgf8*. Genetic analysis suggests that *Tbx1* lies upstream of *Fgf8* in pharyngeal endoderm[46] and also affects *Fgf8* and *Fgf10* expression in SHF mesoderm.[18,46,47] Phenotypic analysis of embryos after tissue specific deletion of *Tbx1* with mesodermal *Cre* lines has shown that mesodermal Tbx1 is critical for SHF and OFT development.[48] This is similar to FGF8[19] and to FGF10 as we now show.

Our findings demonstrate for the first time that mesodermal FGF10, as well as FGF8, is important for formation of the arterial pole of the heart and the PAAs, providing new insight into the cardiovascular abnormalities seen in Di-

George syndrome. Furthermore, mutations in *Fgf10* and *Fgf8* that affect their expression in pharyngeal mesoderm may underlie human congenital heart and vascular defects.

Acknowledgments

We thank Y. Saga for the $MesP1^{Cre/+}$ line and N. Itoh and S. Kato for $Fgf10^{+/-}$ mice. We thank C. Bodin and C. Cimper for help with histology, E. Pecnard and S. Coqueran for genotyping, E.J. Park for scoring of OFT/RV morphology of embryos, and to members of our laboratory and S. Zaffran for helpful discussions.

Sources of Funding

The work performed in the laboratory of M.E.B. was supported by the Institut Pasteur and the Centre National de la Recherche Scientifique, with grants from the European Union Integrated Project "Heart Repair" LHSM-CT2005-018630 (also to R.G.K.) and the CardioCell LT2009-223372 project. The work performed in the laboratory of A.M.M. was supported by the National Institute of Child Health and Development. Y.W. received a fellowship from the European Union Integrated Project "Heart Repair." S.M.-T. received a fellowship from the Naito Foundation to perform work for 6 months in the laboratory of M.E.B.

Disclosures

None.

References

1. Lloyd-Jones D, Adams R, Carnethon M, De Simone G, Ferguson TB, Flegal K, Ford E, Furie K, Go A, Greenlund K, Haase N, Hailpern S, Ho M, Howard V, Kissela B, Kittner S, Lackland D, Lisabeth L, Marelli A, McDermott M, Meigs J, Mozaffarian D, Nichol G, O'Donnell C, Roger V, Rosamond W, Sacco R, Sorlie P, Stafford R, Steinberger J, Thom T, Wasserthiel-Smoller S, Wong N, Wylie-Rosett J, Hong Y. Heart disease and stroke statistics–2009 update: a report from the American Heart Association Statistics Committee and Stroke Statistics Subcommittee. *Circulation.* 2009;119:e21–e181.
2. Nakajima Y, Yamagishi T, Hokari S, Nakamura H. Mechanisms involved in valvuloseptal endocardial cushion formation in early cardiogenesis: roles of transforming growth factor (TGF)-beta and bone morphogenetic protein (BMP). *Anat Rec.* 2000;258:119–127.
3. Webb S, Qayyum SR, Anderson RH, Lamers WH, Richardson MK. Septation and separation within the outflow tract of the developing heart. *J Anat.* 2003;202:327–342.
4. Buckingham M, Meilhac S, Zaffran S. Building the mammalian heart from two sources of myocardial cells. *Nat Rev Genet.* 2005;6:826–835.
5. Franco D, Meilhac SM, Christoffels VM, Kispert A, Buckingham M, Kelly RG. Left and right ventricular contributions to the formation of the interventricular septum in the mouse heart. *Dev Biol.* 2006;294:366–375.
6. Verzi MP, McCulley DJ, De Val S, Dodou E, Black BL. The right ventricle, outflow tract, and ventricular septum comprise a restricted expression domain within the secondary/anterior heart field. *Dev Biol.* 2005;287:134–145.
7. Waldo KL, Hutson MR, Ward CC, Zdanowicz M, Stadt HA, Kumiski D, Abu-Issa R, Kirby ML. Secondary heart field contributes myocardium and smooth muscle to the arterial pole of the developing heart. *Dev Biol.* 2005;281:78–90.
8. Jiang X, Rowitch DH, Soriano P, McMahon AP, Sucov HM. Fate of the mammalian cardiac neural crest. *Development.* 2000;127:1607–1616.
9. Nakamura T, Colbert MC, Robbins J. Neural crest cells retain multipotential characteristics in the developing valves and label the cardiac conduction system. *Circ Res.* 2006;98:1547–1554.
10. Hutson MR, Kirby ML. Model systems for the study of heart development and disease. Cardiac neural crest and conotruncal malformations. *Semin Cell Dev Biol.* 2007;18:101–110.
11. Waldo KL, Hutson MR, Stadt HA, Zdanowicz M, Zdanowicz J, Kirby ML. Cardiac neural crest is necessary for normal addition of the myocardium to the arterial pole from the secondary heart field. *Dev Biol.* 2005;281:66–77.
12. Rochais F, Mesbah K, Kelly RG. Signaling pathways controlling second heart field development. *Circ Res.* 2009;104:933–942.
13. Brown CB, Wenning JM, Lu MM, Epstein DJ, Meyers EN, Epstein JA. Cre-mediated excision of Fgf8 in the Tbx1 expression domain reveals a critical role for Fgf8 in cardiovascular development in the mouse. *Dev Biol.* 2004;267:190–202.
14. Engleka KA, Gitler AD, Zhang M, Zhou DD, High FA, Epstein JA. Insertion of Cre into the Pax3 locus creates a new allele of Splotch and identifies unexpected Pax3 derivatives. *Dev Biol.* 2005;280:396–406.
15. Kelly RG, Brown NA, Buckingham ME. The arterial pole of the mouse heart forms from Fgf10-expressing cells in pharyngeal mesoderm. *Dev Cell.* 2001;1:435–440.
16. Marguerie A, Bajolle F, Zaffran S, Brown NA, Dickson C, Buckingham ME, Kelly RG. Congenital heart defects in Fgfr2-IIIb and Fgf10 mutant mice. *Cardiovasc Res.* 2006;71:50–60.
17. Ryckebusch L, Wang Z, Bertrand N, Lin SC, Chi X, Schwartz R, Zaffran S, Niederreither K. Retinoic acid deficiency alters second heart field formation. *Proc Natl Acad Sci U S A.* 2008;105:2913–2918.
18. Hu T, Yamagishi H, Maeda J, McAnally J, Yamagishi C, Srivastava D. Tbx1 regulates fibroblast growth factors in the anterior heart field through a reinforcing autoregulatory loop involving forkhead transcription factors. *Development.* 2004;131:5491–5502.
19. Park EJ, Ogden LA, Talbot A, Evans S, Cai CL, Black BL, Frank DU, Moon AM. Required, tissue-specific roles for Fgf8 in outflow tract formation and remodeling. *Development.* 2006;133:2419–2433.
20. Ilagan R, Abu-Issa R, Brown D, Yang YP, Jiao K, Schwartz RJ, Klingensmith J, Meyers EN. Fgf8 is required for anterior heart field development. *Development.* 2006;133:2435–2445.
21. Crossley PH, Martin GR. The mouse Fgf8 gene encodes a family of polypeptides and is expressed in regions that direct outgrowth and patterning in the developing embryo. *Development.* 1995;121:439–451.
22. Sun X, Meyers EN, Lewandoski M, Martin GR. Targeted disruption of Fgf8 causes failure of cell migration in the gastrulating mouse embryo. *Genes Dev.* 1999;13:1834–1846.
23. Frank DU, Fotheringham LK, Brewer JA, Muglia LJ, Tristani-Firouzi M, Capecchi MR, Moon AM. An Fgf8 mouse mutant phenocopies human 22q11 deletion syndrome. *Development.* 2002;129:4591–4603.
24. Abu-Issa R, Smyth G, Smoak I, Yamamura K, Meyers EN. Fgf8 is required for pharyngeal arch and cardiovascular development in the mouse. *Development.* 2002;129:4613–4625.
25. Macatee TL, Hammond BP, Arenkiel BR, Francis L, Frank DU, Moon AM. Ablation of specific expression domains reveals discrete functions of ectoderm- and endoderm-derived FGF8 during cardiovascular and pharyngeal development. *Development.* 2003;130:6361–6374.
26. Sekine K, Ohuchi H, Fujiwara M, Yamasaki M, Yoshizawa T, Sato T, Yagishita N, Matsui D, Koga Y, Itoh N, Kato S. Fgf10 is essential for limb and lung formation. *Nat Genet.* 1999;21:138–141.
27. Saga Y, Miyagawa-Tomita S, Takagi A, Kitajima S, Miyazaki J, Inoue T. MesP1 is expressed in the heart precursor cells and required for the formation of a single heart tube. *Development.* 1999;126:3437–3447.
28. Liao J, Aggarwal VS, Nowotschin S, Bondarev A, Lipner S, Morrow BE. Identification of downstream genetic pathways of Tbx1 in the second heart field. *Dev Biol.* 2008;316:524–537.
29. Cai CL, Liang X, Shi Y, Chu PH, Pfaff SL, Chen J, Evans S. Isl1 identifies a cardiac progenitor population that proliferates prior to differentiation and contributes a majority of cells to the heart. *Dev Cell.* 2003;5:877–889.
30. Kelly RG, Papaioannou VE. Visualization of outflow tract development in the absence of Tbx1 using an FgF10 enhancer trap transgene. *Dev Dyn.* 2007;236:821–828.
31. Park EJ, Watanabe Y, Smyth G, Miyagawa-Tomita S, Meyers E, Klingensmith J, Camenisch T, Buckingham M, Moon AM. An FGF autocrine loop initiated in second heart field mesoderm regulates morphogenesis at the arterial pole of the heart. *Development.* 2008;135:3599–3610.
32. Zhang J, Lin Y, Zhang Y, Lan Y, Lin C, Moon AM, Schwartz RJ, Martin JF, Wang F. Frs2alpha-deficiency in cardiac progenitors disrupts a subset of FGF signals required for outflow tract morphogenesis. *Development.* 2008;135:3611–3622.
33. Prall OW, Menon MK, Solloway MJ, Watanabe Y, Zaffran S, Bajolle F, Biben C, McBride JJ, Robertson BR, Chaulet H, Stennard FA, Wise N, Schaft D, Wolstein O, Furtado MB, Shiratori H, Chien KR, Hamada H, Black BL, Saga Y, Robertson EJ, Buckingham ME, Harvey RP. An Nkx2–5/Bmp2/Smad1 negative feedback loop controls heart progenitor specification and proliferation. *Cell.* 2007;128:947–959.
34. Hutson MR, Zhang P, Stadt HA, Sato AK, Li YX, Burch J, Creazzo TL, Kirby ML. Cardiac arterial pole alignment is sensitive to FGF8 signaling in the pharynx. *Dev Biol.* 2006;295:486–497.

35. Mesbah K, Harrelson Z, Theveniau-Ruissy M, Papaioannou VE, Kelly RG. Tbx3 is required for outflow tract development. *Circ Res.* 2008;103: 743–750.
36. Vincentz JW, McWhirter JR, Murre C, Baldini A, Furuta Y. Fgf15 is required for proper morphogenesis of the mouse cardiac outflow tract. *Genesis.* 2005;41:192–201.
37. Aggarwal VS, Liao J, Bondarev A, Schimmang T, Lewandoski M, Locker J, Shanske A, Campione M, Morrow BE. Dissection of Tbx1 and Fgf interactions in mouse models of 22q11DS suggests functional redundancy. *Hum Mol Genet.* 2006;15:3219–3228.
38. Ornitz DM, Xu J, Colvin JS, McEwen DG, MacArthur CA, Coulier F, Gao G, Goldfarb M. Receptor specificity of the fibroblast growth factor family. *J Biol Chem.* 1996;271:15292–15297.
39. Powers CJ, McLeskey SW, Wellstein A. Fibroblast growth factors, their receptors and signaling. *Endocr Relat Cancer.* 2000;7:165–197.
40. Ohuchi H, Hori Y, Yamasaki M, Harada H, Sekine K, Kato S, Itoh N. FGF10 acts as a major ligand for FGF receptor 2 IIIb in mouse multi-organ development. *Biochem Biophys Res Commun.* 2000;277:643–649.
41. Jerome LA, Papaioannou VE. DiGeorge syndrome phenotype in mice mutant for the T-box gene, Tbx1. *Nat Genet.* 2001;27:286–291.
42. Lindsay EA, Vitelli F, Su H, Morishima M, Huynh T, Pramparo T, Jurecic V, Ogunrinu G, Sutherland HF, Scambler PJ, Bradley A, Baldini A. Tbx1 haploinsufficieny in the DiGeorge syndrome region causes aortic arch defects in mice. *Nature.* 2001;410:97–101.
43. Merscher S, Funke B, Epstein JA, Heyer J, Puech A, Lu MM, Xavier RJ, Demay MB, Russell RG, Factor S, Tokooya K, Jore BS, Lopez M, Pandita RK, Lia M, Carrion D, Xu H, Schorle H, Kobler JB, Scambler P, Wynshaw-Boris A, Skoultchi AI, Morrow BE, Kucherlapati R. TBX1 is responsible for cardiovascular defects in velo-cardio-facial/DiGeorge syndrome. *Cell.* 2001;104:619–629.
44. Garg V, Yamagishi C, Hu T, Kathiriya IS, Yamagishi H, Srivastava D. Tbx1, a DiGeorge syndrome candidate gene, is regulated by sonic hedgehog during pharyngeal arch development. *Dev Biol.* 2001;235: 62–73.
45. Vitelli F, Morishima M, Taddei I, Lindsay EA, Baldini A. Tbx1 mutation causes multiple cardiovascular defects and disrupts neural crest and cranial nerve migratory pathways. *Hum Mol Genet.* 2002;11:915–922.
46. Zhang Z, Cerrato F, Xu H, Vitelli F, Morishima M, Vincentz J, Furuta Y, Ma L, Martin JF, Baldini A, Lindsay E. Tbx1 expression in pharyngeal epithelia is necessary for pharyngeal arch artery development. *Development.* 2005; 132:5307–5315.
47. Vitelli F, Taddei I, Morishima M, Meyers EN, Lindsay EA, Baldini A. A genetic link between Tbx1 and fibroblast growth factor signaling. *Development.* 2002;129:4605–4611.
48. Zhang Z, Huynh T, Baldini A. Mesodermal expression of Tbx1 is necessary and sufficient for pharyngeal arch and cardiac outflow tract development. *Development.* 2006;133:3587–3595.

Novelty and Significance

What Is Known?

- FGF8 signaling from pharyngeal ectoderm is required for correct formation of great arteries.
- FGF8 from second heart field mesoderm is required for arterial pole formation.
- *Fgf10*, like *Fgf8*, is expressed in mesodermal cells of the second heart field.
- *Fgf10* mutants have no detectable great artery or arterial pole defects.

What New Information Does This Article Contribute?

- It reveals a new role of FGF10 in formation of the arterial pole of the heart, when FGF8 is reduced or abolished.
- It reveals a previously unexpected role for mesodermal FGF8 function in great vessel development.

More than 30% of congenital heart defects affect development of the arterial pole of the heart. In the mammalian embryo, cells that will contribute to this part of the heart derive from mesoderm of the second heart field. Loss of *Fgf8* function in these cells leads to arterial pole defects. *Fgf10* is also expressed in the second heart field, yet *Fgf10* mutants do not have detectable outflow tract or great vessel defects. This may be attributable to compensation by fibroblast growth factor (FGF)8. To address this question, we examined compound mutants and show that arterial pole defects are more severe in the absence of both *Fgf8* and *Fgf10* function in the second heart field. This is also the case for arch arteries that contribute connecting vessels, such as the subclavian and common carotid arteries, revealing for the first time a role for mesodermal FGF8 and FGF10 in vascular development. Our compound mutant analysis also demonstrates that this requirement is highly dosage sensitive, such that progressive reduction in the number of functional alleles of *Fgf8* and *Fgf10* leads to increasingly severe defects. These findings identify *Fgf8* and *Fgf10* as candidate genes for congenital cardiovascular malformations in the human population.

Supplement Material

Online Method

TUNEL assay and Immunohistochemstry

An In Situ Cell Death Detection Kit (Roche) was used for the TUNEL assay. Phospho-Histone H3 antibody (Cell Signaling Technology #9701), Isl1 (DSHB #39.4D5) and AP2α (DSHB #3B5) antibodies were used for immunohistochemistry.

Online Table I. Number of embryos obtained from *Fgf8$^{flox/+}$;Fgf10$^{+/-}$;MesP1$^{Cre/+}$* x *Fgf8$^{flox/flox}$;Fgf10$^{+/-}$* crosses.

Genotype *Fgf8;Fgf10;Cre*	E9.5	E10.5	E15.5/16.5	E18.5	Expected
flox/+;+/+	6 (3.64%)	4 (3.64%)	4 (5.56%)	4 (7.14%)	6.25%
flox/+;+/-	28 (16.97%)	12 (10.91%)	7 (9.72%)	6 (10.71%)	12.5%
flox/+;-/-	9 (5.45%)	2 (1.82%)	2 (2.78%)	2 (3.57%)	6.25%
flox/flox;+/+	11 (6.67%)	12 (10.91%)	5 (6.94%)	7 (12.5%)	6.25%
flox/flox;+/-	18 (10.91%)	15 (13.64%)	7 (9.72%)	6 (10.71%)	12.5%
flox/flox;-/-	14 (8.48%)	10 (9.09%)	3 (4.17%)	2 (3.57%)	6.25%
Total number	165	110	72	56	

Online Figure legend

Online Figure I. Apoptosis and proliferation in *Fgf8;Fgf10* compound mutants. (A-F) TUNEL assay was performed at E9.5. (A,C) Control *Fgf8$^{flox/+}$;Fgf10$^{+/-}$* embryo shows some cell death in the pharyngeal endoderm (PE) (arrow heads). (B,D) This is increased in the PE and OFT of the *Fgf8$^{flox/flox}$;Fgf10$^{-/-}$* mutant. (A,B) The number of phospho-histone H3 (PHH3) positive cells (arrows) is also less in *Fgf8$^{flox/flox}$;Fgf10$^{-/-}$* mutants (B) compared to control *Fgf8$^{flox/+}$;Fgf10$^{+/-}$* embryos (A). (E,F) Transverse sections at the level of developing fourth PAA in E9.5 embryos show apoptosis in the AP2α-positive cells on the right side of the *Fgf8$^{flox/flox}$;Fgf10$^{+/-}$* mutant (E), but not in control *Fgf8$^{flox/+}$;Fgf10$^{+/-}$* embryos (F). Asterisks indicate the dorsal aorta.

Online Figure I

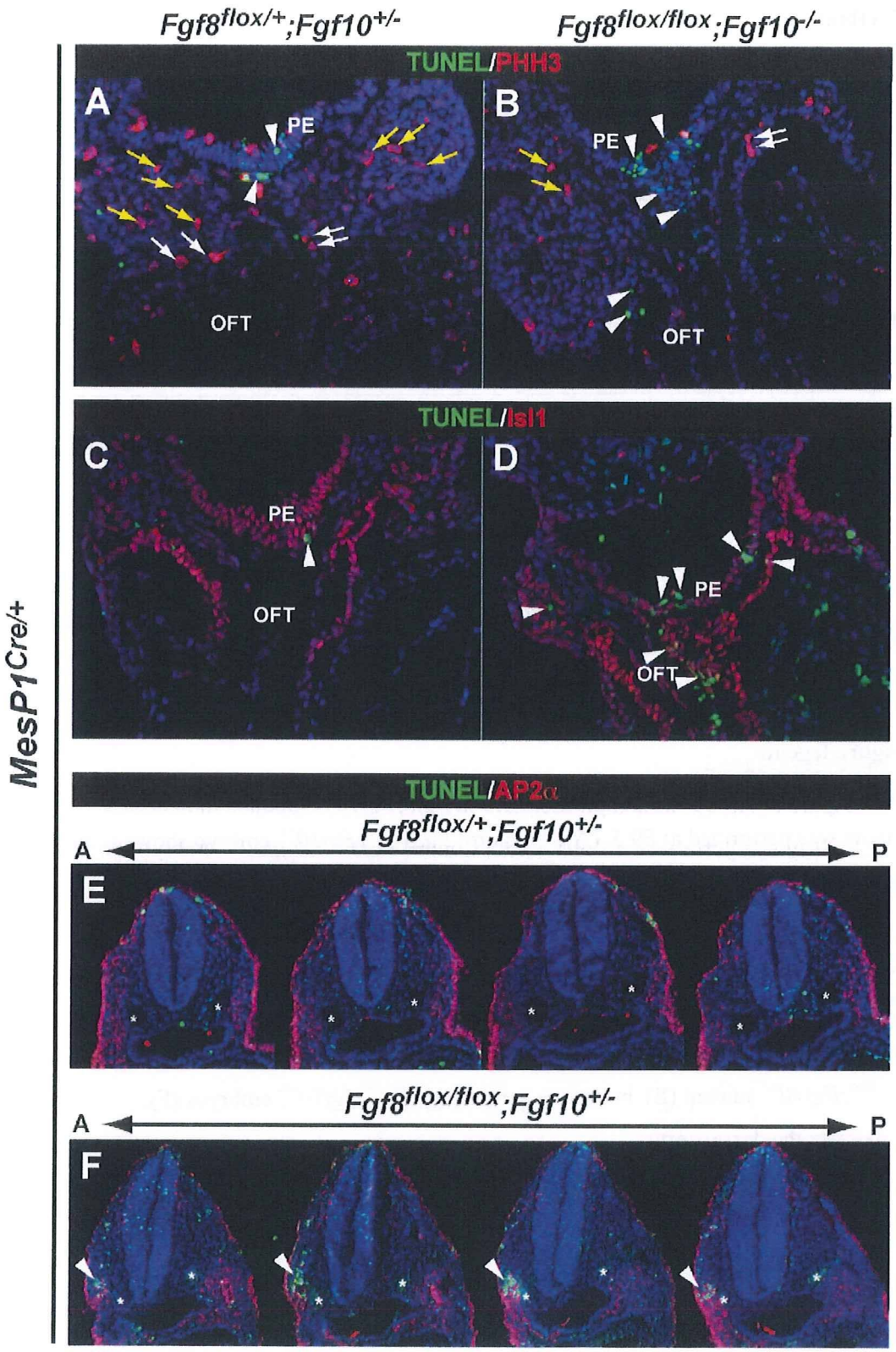

ARTICLE

Spatio-Temporal Dynamics of Gene Expression of the Edn1-Dlx5/6 Pathway During Development of the Lower Jaw

Maxence Vieux-Rochas,[1] Stefano Mantero,[2] Eglantine Heude,[1] Ottavia Barbieri,[3,4] Simonetta Astigiano,[4] Gérard Couly,[1,5] Hiroki Kurihara,[6] Giovanni Levi,[1] and Giorgio R. Merlo[2]*

[1]Evolution des Régulations Endocriniennes, CNRS UMR 7221, Muséum National d'Histoire Naturelle, Paris, France
[2]Dulbecco Telethon Institute, Molecular Biotechnology Center, University of Torino, Torino, Italy
[3]Department of Experimental Medicine, University of Genova, Genova, Italy
[4]Istituto Nazionale per la Ricerca sul Cancro, Genova, Italy
[5]Service de Chirurgie Plastique, Maxillofaciale et Stomatologie, Hôpital Necker-Enfants Malades, Paris, France
[6]Department of Physiological Chemistry and Metabolism, Graduate School of Medicine, University of Tokyo, Tokyo, Japan

Received 26 October 2009; Revised 16 March 2010; Accepted 18 March 2010

Summary: The morphogenesis of the vertebrate skull results from highly dynamic integrated processes involving the exchange of signals between the ectoderm, the endoderm, and cephalic neural crest cells (CNCCs). Before migration CNCCs are not committed to form any specific skull element, molecular signals exchanged in restricted regions of tissue interaction are crucial in providing positional identity to the CNCCs mesenchyme and activate the specific morphogenetic process of different skeletal components of the head. In particular, the endothelin-1 (Edn1)-dependent activation of *Dlx5* and *Dlx6* in CNCCs that colonize the first pharyngeal arch (PA1) is necessary and sufficient to specify maxillo-mandibular identity. Here, to better analyze the spatio-temporal dynamics of this process, we associate quantitative gene expression analysis with detailed examination of skeletal phenotypes resulting from combined allelic reduction of *Edn1*, *Dlx5*, and *Dlx6*. We show that Edn1-dependent and -independent regulatory pathways act at different developmental times in distinct regions of PA1. The Edn1→Dlx5/6→Hand2 pathway is already active at E9.5 during early stages of CNCCs colonization. At later stages (E10.5) the scenario is more complex: we propose a model in which PA1 is subdivided into four adjacent territories in which distinct regulations are taking place. This new developmental model may provide a conceptual framework to interpret the craniofacial malformations present in several mouse mutants and in human first arch syndromes. More in general, our findings emphasize the importance of quantitative gene expression in the fine control of morphogenetic events. genesis 00:1–12, 2010. © 2010 Wiley-Liss, Inc.

Key words: endothelin-1; Dlx; craniofacial development; pharyngeal arches; allelic dosage; cranial neural crest cells; first arch syndromes

INTRODUCTION

Vertebrate jaws are formed through complex morphogenetic processes beginning with the colonization of the first pharyngeal arch (PA1) by *Hox*-negative cephalic neural crest cells (CNCCs) emigrating from the posterior mesencephalic and rhombencephalic neural folds.

Additional Supporting Information may be found in the online version of this article.

Authors' contributions: MV-R carried out mating, pharyngeal arches and skeletal dissections, designed experiments, performed statistical analysis, made figures and prepared the manuscript. SM carried out ISH and quantitative PCR experiments. EH carried out some ISH experiments. OB and SM maintained the animal colony, performed mouse mating and genotyping. GC provided medical expertise and scanners of FAS patients. HK provided Edn1 mutant mice and extensive discussion of the manuscript. GRM carried out ISH, analyzed Real Time PCR data and performed skeletal dissections. GRM and GL designed and coordinated the study, organized the results and prepared the manuscript. All authors read and approved the final manuscript.

Giovanni Levi and Giorgio R. Merlo are co-senior authors.

Abbreviations: CNCCs, cranial neural crest cells; Edn1, endothelin-1; Ednra, endothelin-1 receptor type A; FAS, first arch syndromes; Gsc, goosecoid; PA1, 1st pharyngeal arch; qPCR, quantitative polymerase chain reaction; WT, wild type.

Current address for Maxence Vieux-Rochas: National Research Centre Frontiers in Genetics, School of Life Sciences, Ecole Polytechnique Fédérale (EPFL), Lausanne, Switzerland.

*Correspondence to: Giorgio R. Merlo, Molecular Biotechnology Center, University of Torino, Via Nizza 52, 10126 Torino, Italy.

E-mail: gmerlo@dti.telethon.it

Contract grant sponsors: Telethon Foundation; Cariplo and Compagnia di SanPaolo, Italy; EU Consortium CRESCENDO; French Ministry of Research; Fondation Recherche Médicale; Ministero della Sanità, Italy

Published online in
Wiley InterScience (www.interscience.wiley.com).
DOI: 10.1002/dvg.20625

Whereas CNCCs give rise to most chondrocranial and dermatocranial elements of the jaws (Clouthier *et al.*, 1998; Couly *et al.*, 2002; Depew and Simpson, 2006; Kontges and Lumsden, 1996; Ruhin *et al.*, 2003), they do not possess, before migration, the topographic information needed to carry out the jaw morphogenesis (Couly *et al.*, 1993). Surgical removal and grafting of small territories of the foregut endoderm at different developmental stages has shown that this epithelium provides to CNCCs part of the topographic information needed to form jaw structures (Couly *et al.*, 1993; Kontges and Lumsden, 1996; Kurihara *et al.*, 1994; Le Douarin and Dupin, 2003; Noden and Trainor, 2005; Trainor and Tam, 1995). The molecular nature of the endodermal signals is only partly known, as experimental evidence suggest that FGFs, BMPs, Edn1, and Shh are surely involved (Benouaiche *et al.*, 2008; Ozeki *et al.*, 2004; Vieux-Rochas *et al.*, 2007).

In this study, we have analyzed mice with combined and/or partial loss of *Edn1* and *Dlx5;Dlx6* alleles. The Edn1→Dlx5/6→Hand2 signaling is a relevant model to study the spatio-temporal dynamics of gene expression in the PA1 and the consequences for CNCCs specification. Indeed *Edn1* is expressed in the endoderm and in the mesodermal core of the mandibular prominence of PA1, whereas *Ednra* (*Edn1 receptor-type A*) is broadly expressed by the CNCC-derived PA1 ectomesenchyme and *Dlx5;Dlx6* are only expressed in the mesenchyme of the mandibular prominence (Abe *et al.*, 2007; Clouthier *et al.*, 1998, 2000; Ozeki *et al.*, 2004; Ruest *et al.*, 2004, 2005). Loss of Edn1→Ednra signaling results in the down regulation of the two members of the *distalless* homeobox gene family *Dlx5* and *Dlx6* (Merlo *et al.*, 2002a; Panganiban and Rubenstein, 2002), and in a homeotic-like transformation of lower into upper jaw structures, similar to that observed upon double inactivation of *Dlx5* and *Dlx6* (Beverdam *et al.*, 2002; Depew *et al.*, 2002; Fukuhara *et al.*, 2004; Ruest *et al.*, 2004). The constitutive activation of the Edn1→Ednra signaling in the entire PA1 induces a partial transformation of the upper jaw suggesting that PA1 CNCCs are competent to respond to Edn1 signaling.

Within the PA1 of E10.5 mouse embryos *Dlx* genes are expressed in nested proximo/distal domains: *Dlx1* and *Dlx2* in the proximal and distal maxillary and mandibular prominences, *Dlx5* and *Dlx6* in the entire mandibular prominence, while *Dlx3* only in a medio/distal territory of the mandibular prominence (Depew *et al.*, 2002; Merlo *et al.*, 2000). The most informative data on the role of *Dlx* genes in PA1 patterning come from the analysis of mice carrying single or multiple inactivating mutations for *Dlx1*, *Dlx2*, *Dlx5*, and *Dlx6*. In *Dlx5;6* double mutant mice, lower jaw cartilages and bones are transformed and acquire the shape typical of upper jaw elements. Furthermore, in *Dlx5;6* double null mice, *vibrissae* and palatine rugae are symmetrically present in the upper and lower jaw, suggesting that an homeotic transformation has taken place (Beverdam *et al.*, 2002; Depew *et al.*, 2002). In Dlx1;2 double null mice the proximal maxillary region develops abnormal skeletal elements reminiscent of the reptilian upper jaw (Depew *et al.*, 2005; Qiu *et al.*, 1997). These observations have led to the proposition that the combinatorial expression of Dlx genes by PA1 CNCCs determine their relative position and their capacity to give rise to different skeletal elements (Depew and Simpson, 2006; Depew *et al.*, 2005; Merlo *et al.*, 2000).

Several genes have been shown to act downstream of *Dlx5* and *Dlx6*, including *Gsc*, *Pitx1*, *Wnt5a*, *Dlx3*, *Meis2*, and the bHLH transcription factor *Hand2* (Beverdam *et al.*, 2002; Depew *et al.*, 1999, 2002; Merlo *et al.*, 2000, 2002a). A further set of candidate targets of Dlx5/6 have been recently identified (Jeong *et al.*, 2008). Several of the proposed targets might be directly regulated by Dlx5/6 (e.g., *Gbx2, Hand2*) as their promoters harbor Dlx-binding regulatory elements (Charite *et al.*, 2001; Jeong *et al.*, 2008).

Integrating quantitative gene expression data with observed phenotypes we propose that Edn1 signaling occurs in two phases: (1) early in development, Edn1 activates the *Dlx5/6→Hand2* pathway in postmigratory CNCCs. (2) Late in development, distinct regulations can be recognized in distinct regions of the mandibular prominence: in a more proximal region *Dlx5/6* are activated independently from Edn1 and their expression is not associated with *Gsc*. More distally *Dlx5/6* expression depends on Edn1 signaling and results in the activation of downstream genes including *Gsc* and *Pitx1*. *Hand2* is expressed only in the medio/distal region of the mandibular prominence and its expression depends upon at least three different, regionally restricted, regulations. We conclude that the organization of latero/proximal PA1 structures depends on the quantitative, gene-dosage dependent, regulation of the Edn1→Dlx5/6→(Gsc, Pitx1, etc...) pathway, while medio/distal lower jaw morphology depends on *Hand2* expression. Our findings may also provide the developmental framework in which to elucidate and functionally characterize the molecular lesions, yet to be identified, causing or associated with those human first arch syndromes (FAS) affecting the proximal arch.

RESULTS

Edn1 Allelic Dosage and Dynamics of *Dlx* and *Hand2* Expression in PA1

To better define the role of Edn1/Ednra signaling in the control of mandibular morphogenesis, we examined the effects of allelic reduction of *Edn1* on the expression of key regulators of PA1 patterning. First, we measured by RT-qPCR the abundance of *Dlx2, 3, 5, 6*, and *Hand2* transcripts in the dissected mandibular prominence (the ventral segment of the PA1) of WT and $Edn1^{+/-}$ E9 embryos. At this stage of development CNCCs are still migrating, but most of them have already colonized the mandibular region (Couly *et al.*, 2002; Couly *et al.*, 1993; Le Douarin *et al.*, 2004). In $Edn1^{+/-}$ mandibular

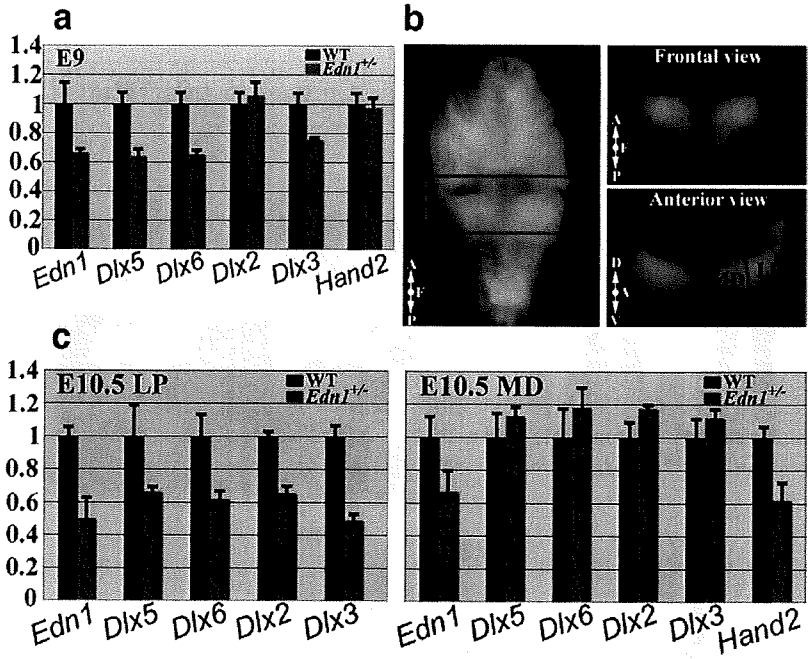

FIG. 1. Effects of allelic reduction of *Edn1* on *Dlx* and *Hand2* gene expression levels in PA1 at E9 and E10.5. (**a**) RT-qPCR measurement of mRNA abundance of *Edn1, Dlx5, Dlx6, Dlx2, Dlx3* and *Hand2* in mandibular prominences from WT (black bars) or $Edn1^{+/-}$ (red bars) at E9. (**b**) Dissection procedure used to separate the LP from the MD part of the mandibular prominence of PA1 at E10.5. The whole mandibular process was first isolated from the embryo and the latero-proximal and medio-distal portions were then separated with a single sharp cut (red line). (**c**) Quantification of the mRNA abundance of *Edn1, Dlx5, Dlx6, Dlx2, Dlx3*, and *Hand2* in LP (left) and MD (right) dissected mandibular prominences from WT (black bars) or $Edn1^{+/-}$ (red bars) at E10.5. WT is set = 1. Axis orientation: A, anterior; D, dorsal; F, frontal; P, posterior; V, ventral. LP, latero-proximal; MD, medio-distal. Black bars represent standard deviation between two independent samples.

prominences, *Edn1* expression was reduced by 38% compared to WT, while *Dlx5, Dlx6*, and *Dlx3* levels were reduced respectively of 35, 36, and 24%. *Dlx2* and *Hand2* were virtually unchanged (Fig. 1a).

Then, we carried out a similar analysis on dissected mandibular prominences obtained from E10.5 WT and $Edn1^{+/-}$ embryos. In this case we further subdivided the mandibular prominence into a latero/proximal (LP) and a medio/distal (MD) segment (as shown in Fig. 1b). In the LP segment, *Dlx2, Dlx3, Dlx5*, and *Dlx6* levels were reduced by 35, 50, 35, and 39%, respectively; *Hand2* expression was very low and was therefore not considered. In the MD segment the levels of expression of *Dlx2*, *Dlx3*, *Dlx5*, and *Dlx6* were not detectably different, while *Hand2* transcripts were reduced by 40% (Fig. 2b). In the LP and MD segments of $Edn1^{+/-}$ mandibular prominences, *Edn1* transcripts were reduced, respectively by 60 and 40% (Fig. 1c).

Thus, loss of one *Edn1* allele reduces the expression levels of *Dlx* genes in E9 mandibular prominences while at E10.5 *Dlx* expression is only reduced in the LP part of the mandibular prominence but not in the MD. However, in the MD portion of the E10.5 mandibular prominence, *Hand2* expression is detectably reduced, suggesting that Edn1 can regulate *Hand2* expression independently from *Dlx* genes.

Expression of *Dlx* Target Genes in the Mandibular Prominence of *Dlx5;Dlx6* Mutant Embryos

In different regions of the mandibular prominence of PA1 Edn1 and Dlx5/6 signaling could act independently. This led us to analyze the quantitative effects of *Dlx5/6* allelic reduction. We first examined how the loss of *Dlx5;Dlx6* alleles affected their own level of mRNA expression. In the mandibular prominence of $Dlx5^{+/-}$;$Dlx6^{+/-}$ embryos *Dlx5* and *Dlx6* mRNAs were reduced, respectively, by 40 and 45%, while in that of $Dlx5^{-/-}$;$Dlx6^{-/-}$ embryos *Dlx5* and *Dlx6* mRNAs were nearly undetectable (Fig. 2a). To further confirm this finding, we performed in situ hybridization. In $Dlx5^{+/-}$;$Dlx6^{+/-}$ embryos we observed a reduced *Dlx5* and *Dlx6* signal in the first and second PA, and in the otic vesicle (Fig. 2b). These results confirm that each allele contributes to the pool of transcripts and that mRNA abundance directly reflects allele dosage.

It has been shown that in the mandibular prominence of $Dlx5^{-/-}$;$Dlx6^{-/-}$ embryos, the expression of many target genes is either up- or down-regulated (Beverdam *et al.*, 2002; Depew *et al.*, 2002; Jeong *et al.*, 2008); in particular it appears that Dlx6 directly activates the transcription of *Hand2* by binding at its promoter (Charite *et al.*, 2001). We determined the expression level of putative *Dlx5;Dlx6* target genes on whole PA1s and on dissected LP and MD segments from embryos with different *Dlx5;Dlx6* allelic

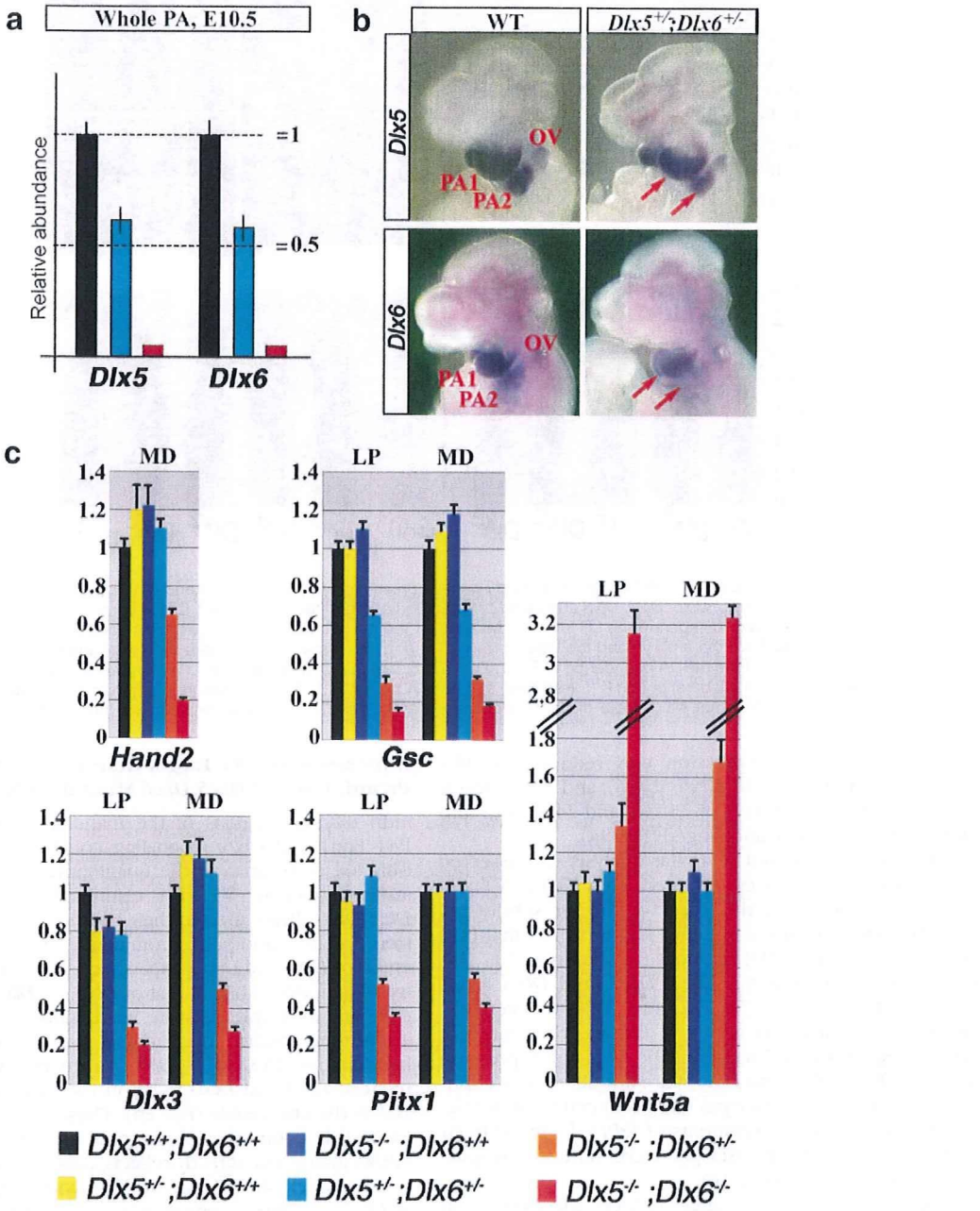

FIG. 2. Effect of allelic reduction of *Dlx5* and *Dlx6* on gene expression levels of target genes in PA1 at E10.5. (**a**) RT-qPCR measurement of *Dlx5* and *Dlx6* transcripts abundance in PA1 of E10.5 WT (black bars), $Dlx5^{+/-};Dlx6^{+/-}$ (blue bars) or $Dlx5^{-/-};Dlx6^{-/-}$ (red bars) embryos. The WT is set = 1, standard deviation is reported. (**b**) In situ hybridization with *Dlx5* (top) and *Dlx6* (bottom) probes on E10.5 WT (left) and $Dlx5^{+/-};Dlx6^{+/-}$ (right) embryos, showing reduction in mRNA levels in the PAs and otic vesicle of heterozygous embryos. (**c**) PA1s were dissected from E10.5 embryos with progressive loss of *Dlx5* and *Dlx6* alleles and further divided into LP and MD regions (see Fig. 1), and stored individually. Samples of similar genotype were pooled. The levels of expression of the *Dlx* targets *Hand2, Pitx1, Dlx3, Gsc*, and *Wnt5a* were measured by RT-qPCR. The results are color-coded by the number of absent *Dlx* alleles. WT is set = 1.

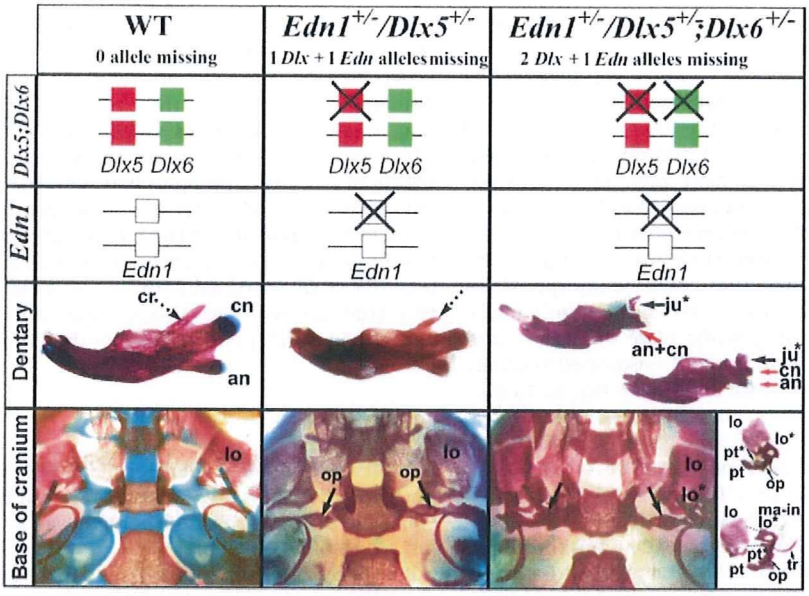

FIG. 3. Allelic reduction of *Dlx5;Dlx6* and *Edn1* results in specific proximal defects. WT, $Edn1^{+/-}/Dlx5^{+/-}$ and $Edn1^{+/-}/Dlx5^{+/-};Dlx6^{+/-}$ newborn mice. Loss of one *Dlx* and one *Edn1* allele results in reduction of the coronoid process of the dentary (dashed arrows) and in the appearance of an extra bone between the pterygoid bone and the middle ear (*os paradoxicum*; green arrows). In $Edn1^{+/-}/Dlx5^{+/-};Dlx6^{+/-}$ mice (right), we observe fusion of the condylar and angular processes (red arrows) of the dentary bone; appearance of duplicated jugal bones in the proximal mandibular arch (black arrows) and the appearance of the *os paradoxicum* (green arrows). Note also the appearance of duplicated structures (asterisks) in the lamina obturans/pterygoid region of the base of the cranium, (further dissociated and shown on the right). *Abbreviations*: an, angular process; cn, condylar process; cr, coronoid process; ds, dentary-squamosal articulation; ju, jugal bone; LO, Lamina Obturans; op, *os paradoxicum*; pt, pterygoid; tb; tympanic bone; tr, tympanic ring; zy, zygomatic arch.

dosage (Fig. 2c, Supporting Information Fig. 1). Both up- (*Wnt5a, Meis2*) and down-regulated (*Hand2*, *Pitx1*, *Dlx3*, and *Gsc*) transcripts were examined.

Similar regulations were observed in the LP and MD subregions, with the exception of *Hand2* whose expression in LP was very low and could not be analyzed by RT-qPCR. Allelic reduction of only one or two *Dlx5/6* alleles did not have detectable effects with the exception of *Gsc*, which was reduced of 35% in both LP and MD regions. Inactivation of three out of four *Dlx5/6* alleles ($Dlx5^{-/-};Dlx6^{+/-}$) resulted in more pronounced regulations: *Hand2* (−35%), *Pitx1* (−45%), *Dlx3* (−50%), *Gsc* (−65%), and *Wnt5a* (+170%). In $Dlx5^{-/-};Dlx6^{-/-}$ embryos: *Hand2* was reduced of 80%, *Pitx1* of 60%, *Dlx3* of 75% *Gsc* of 85% while *Wnt5a* was increased three folds (Fig. 2c). *Meis2* expression was slightly increased (+30%) in the PA1 of $Dlx5^{-/-};Dlx6^{-/-}$ embryos (Supporting Information Fig. 1a) but did not change in all the other genotypes.

The progressive reduction in mRNA abundance of *Hand2* and *Dlx3* in the mandibular prominence of embryos with three or four *Dlx5/6* alleles missing was verified by in situ hybridization. While in $Dlx5^{-/-};Dlx6^{-/-}$ embryos *Hand2* and *Dlx3* expression was below detection, in $Dlx5^{-/-};Dlx6^{+/-}$ embryos we observed a reduced hybridization signal compared to WT embryos (Supporting Information Fig. 1b). These findings suggest that a threshold level of *Dlx5* and *Dlx6* mRNA is necessary to activate target gene transcription.

Craniofacial Phenotypes of Mice With Combined Loss of *Edn1* and *Dlx5;Dlx6* Alleles

Dlx and *Hand2* genes play important roles in the control of craniofacial morphogenesis. As the loss of one *Edn1* allele reduces the expression levels of *Dlx* and *Hand2* genes, we analyzed the skulls of $Edn1^{+/-}$ newborn mice, but no obvious malformation could be detected (not shown); this finding is not surprising as $Dlx2^{+/-}$, $Dlx5^{+/-}$, $Dlx5^{+/-}$; $Dlx6^{+/-}$ and $Hand2^{+/-}$ mice also show only minor craniofacial defects (Acampora *et al.*, 1999; Beverdam *et al.*, 2002; Depew *et al.*, 1999; Robledo *et al.*, 2002; Yanagisawa *et al.*, 2003). As the loss of one *Edn1* allele could further reduce the level of *Dlx5/6* and/or *Hand2* expression, we examined the craniofacial skeleton of combined *Edn1/Dlx* mutant mice. We therefore crossbred $Edn1^{+/-}$ mice with either $Dlx5^{+/-}$ or $Dlx5^{+/-};Dlx6^{+/-}$ mice.

When both one *Edn1* and one *Dlx5* allele were lost, we observed a slightly shorter coronoid process of the dentary and the appearance of an *os paradoxicum* at the base of the cranium, highly reminiscent of that observed in $Dlx5^{+/-};Dlx6^{+/-}$ or in $Dlx5^{-/-}$ or $Dlx6^{-/-}$ mutants; in each of these allelic configurations two *Dlx5/6* alleles are missing (Fig. 3, Supporting Informa-

tion Fig. 4 and Table 1; Jeong *et al.*, 2008). No other obvious defect was observed.

In *Edn1*$^{+/-}$/*Dlx5*$^{+/-}$;*Dlx6*$^{+/-}$ mice we observed a more severe phenotype. The distance between the condylar and angular processes of the dentary was reduced and often these two processes fused into a single large structure, similar to the zygomatic process of the maxilla. The coronoid process was missing and an additional skeletal element was often observed between the abnormal condylar process (lower jaw) and the jugal bone (upper jaw). This new structure could be interpreted as a duplicated jugal bone. At the base of the cranium, the pterygoid and the *ala temporalis* were duplicated and fused with the *os paradoxicum* and positioned ventrally to overlap with the normal structure (see Fig. 3). Collectively, these phenotypes closely resemble those observed in *Dlx5*$^{-/-}$;*Dlx6*$^{+/-}$ animals (three *Dlx* alleles missing; Supporting Information Fig. 2; Beverdam *et al.*, 2002; Depew *et al.*, 2005). Indeed *Dlx5*$^{-/-}$;*Dlx6*$^{+/-}$ mice also display reduced distance or fusion of the condylar and angular processes of the dentary and the lateral extension of the fused processes giving rise to a structure similar to the zygomatic process of the maxilla. In these mice an extra element is also present, which can be interpreted as a duplicated jugal bone and duplication of the pterygoid-ala temporalis-lamina obturans on the mandibular side. Thus, the anomalies seen in *Dlx5*$^{-/-}$;*Dlx6*$^{+/-}$, and in *Edn1*$^{+/-}$/*Dlx5*$^{+/-}$;*Dlx6*$^{+/-}$ newborns affect derivatives of the proximal region of the mandibular segment, while derivatives of the distal region such as the body of the dentary show no major defects. In most embryos these defects were asymmetric, namely the left side of the mandible was more severely affected than the right one (data not shown). In summary: (1) the gradual changes observed in the levels of expression of Dlx5/6 targets correlate well with the progressive onset of specific skeletal anomalies affecting the proximal lower jaw and 2) the reduction of *Edn1* level of transcription, in combination with the loss of one or two *Dlx5;Dlx6* alleles, has phenotypic consequences similar to the loss of one additional *Dlx* allele (Figs. 2 and 3, and Supporting Information Fig. 3).

Remarkably, the defects caused by allelic reduction of *Edn1* and *Dlx5;Dlx6* resemble those present in patients affected by first arch syndromes (FAS) in which only proximal derivatives of PA1 are affected and which often show the presence of ectopic bones positionally homologous to a duplicated jugal (see Discussion).

Effect of *Ednra* and *Dlx5/6* Inactivation on Downstream Targets Expression Pattern

In the mandibular prominence of normal E10.5 embryos, *Dlx5* and *Dlx6* are expressed in a large and coherent territory extending distally from a proximal limit corresponding to the maxillo/mandibular boundary. The distal-most region of PA1, including the medial fusion, does not, however, express *Dlx5* and *Dlx6* (Fig. 4a,c,e,g). Inactivation of *Ednra* completely prevents the expression of *Dlx5* and *Dlx6* in the E9.5 PA1 (Ozeki *et al.*, 2004); in these same mutants at E10.5, however, *Dlx5* and *Dlx6* are expressed in an Edn1-independent territory in the proximal part of PA1 (Fig. 4b,d,f,h black arrows; Ozeki *et al.*, 2004). In normal E10.5 embryos, *Gsc* expression is limited to a distal region of PA1 overlapping in part with the Edn1-dependent territory of *Dlx* activation. *Gsc* expression is abolished in both *Ednra* and *Dlx5/6* mutant mice (Fig. 4i–n). Careful analysis of our embryos revealed an additional territory of *Gsc* expression in the proximal endoderm of PA1 (red arrows, Fig. 5i–k,n), this small territory of expression is independent from both Ednra and Dlx5/6.

DISCUSSION

An emerging theme in developmental biology is the importance of quantitative functions shared by related and coexpressed genes. Examples of these are the signaling functions of FGFs expressed in the apical ectodermal ridge (Mariani *et al.*, 2008), the gene-dosage dependent functions of *Msx1* and *Msx2* for osteogenic differentiation of CNCCs (Han *et al.*, 2007), and the progressive limb phenotypes associated with the combined loss of posterior *HoxD* alleles and with a gradual increase of expression of the HoxD target Epha3 (Cobb and Duboule, 2005). Our study offers a new example in this direction. One implication of this is that the function of individual genes is best examined upon partial and cumulative gene losses, and within the context of expression of related genes. Indeed, the examination of developmental phenotypes in mice homozygous for recessive mutant mice, although widely used, has serious limitations. One of these is the inability to recognize late-occurring regulations (or phenotypes), in case an early event severely affects morphogenesis, patterning or embryonic viability. Second, we cannot appreciate the phenotypic consequences of reduced gene expression; third we may fail to recognize the dynamics of cell–cell signaling and interactions, as these often require a nearly normal context. Such is the case of Edn1→Dlx signaling at the basis of the homeotic lower jaw transformation, to investigate which many studies have been carried out based on either loss-of-function (Acampora *et al.*, 1999; Beverdam *et al.*, 2002; Clouthier *et al.*, 1998; Depew *et al.*, 1999, 2002; Kurihara *et al.*, 1994; Ozeki *et al.*, 2004; Sato *et al.*, 2008a; Thomas *et al.*, 1998; Yanagisawa *et al.*, 2003) or gain-of-function mutants (Sato *et al.*, 2008b). Here we provide quantitative data on the effects of allelic reduction of *Edn1* and *Dlx5;Dlx6* at different developmental stages. Our findings are complementary to those recently reported by Ruest and Clouthier (2009) using CNCC-specific gene deletion and receptor antagonism, and corroborate and extend their major conclusions. We show that, during PA1 development, different Edn1-dependent regulatory pathways act at diverse developmental times in distinct regions of the mandibular prominence. We also show that upon partial

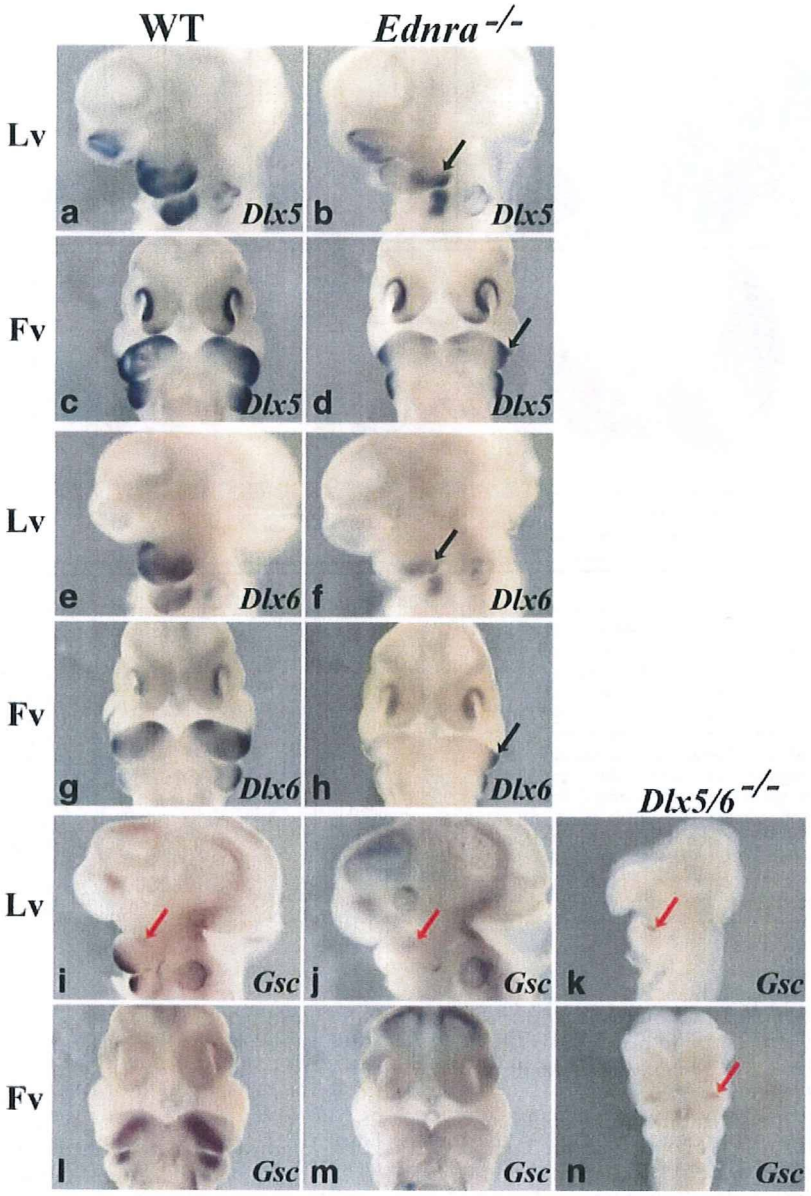

FIG. 4. *Dlx5, Dlx6* and *Gsc* expression in *Ednra* and *Dlx5/6* mutant mice. Whole-mount in situ hybridization on wild-type (**a,c,e,g,i,l**), *Ednra*$^{-/-}$ (**b,d,f,h,j,m**) or *Dlx5/6*$^{-/-}$ (**k,n**) E10.5 embryos using *Dlx5* (a–d), *Dlx6* (e–h) and *Gsc* (i–n) probes. *Dlx5* and *Dlx6* are expressed in the mandibular part of the PA1 and in the PA2 of wild-type embryos (a,b,e,f). In Ednra homozygous mutants, distal expression of *Dlx5* and *Dlx6* is lost in PA, but is still maintained in the proximal part of PA1 (black arrow) and PA2 (c,d,g,h). In normal embryos, *Gsc* is expressed in a latero-distal region within PA1 and PA2 and in a small endodermal territory located at the mandibulo-maxillary junction (red arrow) (i,l). In *Ednra* and *Dlx5/6* mutant embryos, *Gsc* expression is lost in the distal PA1 and PA2 whereas is still maintained in the endoderm at the mandibulo-maxillary junction (j–n). Fv, Frontal view; Lv, Lateral view.

allele loss, the proximal territory of mandibular prominence is the region mainly affected.

At early stages of CNCCs colonization, Edn1 signaling activates *Dlx5/6* expression in CNCCs; accordingly *Dlx5/6* mRNAs are reduced at E9 in the mandibular prominence of *Edn1* heterozygotes (see Fig. 1). If early Edn1 signaling is abrogated (i.e., in *Edn1* or *Ednra*-null mice), *Dlx5/6* fail to be activated in the entire PA1 at least up to E9.5 (Abe *et al.*, 2007; Ozeki *et al.*, 2004; see Fig. 5). This implies that signals that pattern *Dlx* expres-

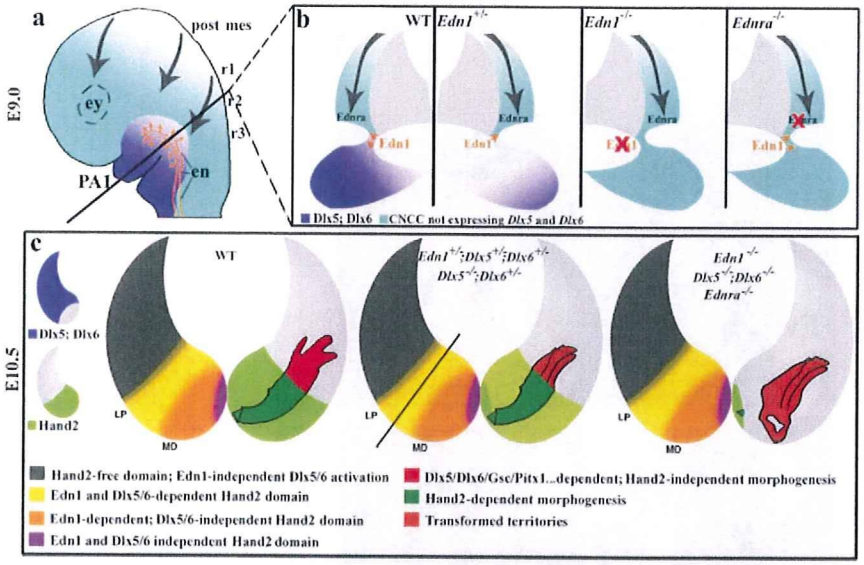

FIG. 5. Summary diagram of Edn1-dependent regulations occurring during PA1 development and hypothetical model for the origin of first arch syndromes. **(a)** Schematic view illustrating CNCCs migration on a lateral view of an E9 mouse embryo. In orange is indicated the endoderm from which *Edn1* signaling originates, in purple the postmigratory CNCCs expressing *Dlx5/6*, in light blue the territory of migration of CNCCs (arrows). **(b)** Drawings represent transverse sections through the embryo in (A), the same color code is used. Sections corresponding to WT, *Edn1*$^{+/-}$, *Edn1*$^{-/-}$ and *Ednra*$^{-/-}$ embryos are shown. Note the reduced level of *Dlx5/6* in *Edn1*$^{+/-}$ embryos and the absence of early *Dlx5/6* activation when Edn1 signaling is disrupted. **(c)** Summary scheme representing different modes and territories of gene activation in E10.5 mandibular prominence. Small inserts on the left represent the territories of expression of *Dlx5/6* (upper, purple) and *Hand2* (lower, light green) respectively in WT embryos. The diagram on the left represents the frontal view of the mandibular part of PA1 of a WT E10.5 embryo. The central diagram refers to three *Dlx/Edn1* alleles missing, either *Dlx5*$^{-/-}$;*Dlx6*$^{+/-}$ or *Edn1*$^{+/-}$/*Dlx5*$^{+/-}$;*Dlx6*$^{+/-}$. Finally the right diagram refers to homozygous mutants for either *Edn1*, *Ednra* or *Dlx5/6*. The color code used in the left side of each drawing indicates the four different regulations observed in PA1 at this stage and are detailed in the caption of this panel. The large grey area corresponds to the Hand2-independent part of PA1, while in all colored, distal regions Hand2 regulation is important for correct morphogenesis. The right part of the diagram depicts the levels of *Hand2* expression encountered in the different mutants as well as the morphogenetic defects occurring in the proximal and distal part of the dentary. The subdivisions of different regions of the mandibular prominence are not divided by actual borders, but represent partially overlapping expression/regulation territories. Color-coded region have faded borders to indicate this. *Abbreviations*: en, endoderm; ey, eye; LP, latero proximal; MD, medio-distal; post mes, posterior mesenchephalon; r1, rhombomere 1; r2, rhombomere 2; r3, rhombomere 3.

sion, such as Edn1 or FGF8 likely act on CNCCs prior to E10.5; for example *Dlx5* expression in response to Edn1 initiates around E8.5-E9 in CNCCs migrating to the distal PA1 (Vieux-Rochas *et al.*, 2007).

At later stages (E10.5) the situation is more complex. Combining our data with results reported in the literature, we propose a model in which the E10.5 mandibular arch is subdivided into four adjacent territories, in which distinct timing and patterns of gene expression are linked to the onset of specific phenotypes (Fig. 5c): (1) in the distal-most region (purple in Fig. 5c), *Hand2* expression is independent from both Edn1 and Dlx5/6. Indeed, *Hand2* expression is retained in a small distal territory in *Edn1*-null, *Ednra*-null and *Dlx5;6*-null animals (Beverdam *et al.*, 2002; Clouthier *et al.*, 2000; Fukuhara *et al.*, 2004; Ozeki *et al.*, 2004; Ruest *et al.*, 2004), possibly associated with the specific fate of this region to undergo midline fusion (Barbosa *et al.*, 2007). (2) in the MD region of PA1, *Hand2* expression can be activated by Edn1 independently of Dlx5/6 as seen from the fact that *Edn1* allelic reduction affects *Hand2*, but not *Dlx5/6* expression (see Fig. 1). This Dlx-independent *Hand2* regulation could well take place in the distal Dlx5/6-free region of the E10.5 PA1 (orange in Fig. 5c). (3) In the medial region of PA1 at E10.5 (yellow in Fig. 5c), *Hand2* is activated through the established Edn1→Dlx6 pathway most probably involving the reported Dlx6-dependent *Hand2* enhancer (Charite *et al.*, 2001). Notably, inactivation of this enhancer results in defects in the medio-distal part of PA1 as suggested by our model (Yanagisawa *et al.*, 2003) and by timed inhibition of Edn1 signaling using Ednra antagonists (Ruest and Clouthier, 2009). (4) Finally, in the proximal part of the E10.5 PA1 (grey in Fig. 5c), *Hand2* is never expressed. Within subterritories of this same region *Dlx5* and *Dlx6* can be activated even in the absence of an Edn1 inducing signal. These different sub-territories could confer a regional selectivity, in turn required for the correct unfolding of the lower jaw morphogenetic program.

Allelic reduction of *Edn1* results in lower *Dlx5/Dlx6* (and *Dlx2* and *Dlx3*) expression in the proximal, but not

in the medio-distal part of the mandibular prominence at E10.5. Therefore, the expression of *Dlx* genes in the distal PA1 (at early stages) is independent from Edn1. A possible interpretation of these findings is that an initial Edn1 signal is necessary to activate *Dlx5/6* expression in incoming CNCCs and that, at later stages, the distal expression of these genes is maintained independently of Edn1 (Fig. 1c). In support of this, Dlx5/6 expression in the proximal PA1 is reactivated at E10.5 even in the absence of Edn1 (Fig. 5a–h; Ozeki *et al.*, 2004), indicating the existence of an Edn1-independent mechanism of *Dlx5/6* activation or maintenance in the LP region. The reduced expression of *Dlx2* and *Dlx3* in the presence of only one *Edn1* allele may indicate the possibility of a global Edn1→Dlx control, or of Dlx5;6 regulating the expression of *Dlx2* and *Dlx3*. This hypothesis, however, would need to be specifically tested.

Allelic reduction of *Edn1* affects *Hand2* expression in the MD territory suggesting an Edn1-dependent, Dlx-independent regulation of *Hand2* which might take place in the Dlx-free region of the distal PA1. Hand2 is expressed in the distal mandibular prominence and its inactivation causes loss of distal skeletal elements of the lower jaw (Yanagisawa *et al.*, 2003). Analysis of the regulatory regions of *Hand2* has revealed the presence of an *Edn1*-responsive enhancer whose activation depends upon binding of Dlx6, although other, yet unspecified, Edn1-dependent proteins could bind to this enhancer (Charite *et al.*, 2001). On the basis of these results, it has been proposed that Hand2 is the final effector of the Edn1→Dlx5/6 regulatory cascade and its level of expression could determine the shape of the distal lower jaw (Sato *et al.*, 2008b; Yanagisawa *et al.*, 2003). However, targeted inactivation of the Edn1/Dlx6-dependent enhancer does not completely abrogate *Hand2* expression in the distal part of PA1 suggesting that other, not yet identified, regulatory elements might activate *Hand2* expression in PA1 (Yanagisawa *et al.*, 2003). As *Hand2* is expressed only in the medio-distal portion of PA1 while *Edn1*, *Ednra* and *Dlx* genes are expressed both in proximal and distal parts of PA1 an active suppression mechanism for *Hand2* expression might be acting in the proximal territory.

Considering *Hand2* expression and regulation, and the loss of the distal lower jaw in Hand2 null mice (Thomas *et al.*, 1998; Yanagisawa *et al.*, 2003), we conclude that the mandibular arch is subdivided into two Hand2-independent and dependent parts corresponding to the proximal and distal part of the dentary, respectively. This notion is supported by the fact that, forced expression of *Hand2* in the whole PA1, including the maxillary arch, induces only transformation of maxillary derivatives into distal mandibular structures (Sato *et al.*, 2008b).

The phenotypes of mice carrying combined *Dlx* gene mutations, and the nested expression of *Dlx* genes within the PAs at E10.5 have led to the proposal that *Dlx* genes might establish maxillo-mandibular identity by providing a *Hox*-like proximo/distal and upper/lower combinatorial code (Depew *et al.*, 2002, 2005). A more sophisticated model, known as the "hinge-caps" organization of the PA1, has been proposed (Depew and Compagnucci, 2008). Both of these models, however, do not take in account the dynamics of gene expression and cell migration during PA1 development. In our view, the nested *Dlx* gene expression pattern is likely to be the consequence of patterning events occurring at much earlier stages, as by E10.5 most CNCCs have already migrated to their final position, have initiated expression of PA-specific genes and are fate-committed (Couly *et al.*, 1998; Le Douarin *et al.*, 2004; Le Douarin and Dupin, 2003).

CNCCs of the proximal mandibular prominence appear more sensitive to variations in the genetic environment, than are distal ones: inactivation or allelic reductions of *Edn1, Ednra, Dlx5* (Acampora *et al.*, 1999; Depew *et al.*, 1999), *Dlx6* (Jeong *et al.*, 2008), *Gsc* (Yamada *et al.*, 1995), *Pitx1* (Bobola *et al.*, 2003; Lanctot *et al.*, 1999), *Gbx2* (Byrd and Meyers, 2005) all lead to proximal defect of the dentary or of the middle and external ear whereas derivatives of the distal part of the first arch are not affected. Interestingly, *Dlx5;Dlx6* are expressed at higher level distally (Figs. 2 and 4) and even allelic reduction of *Edn1* results in maintaining their distal expression levels. These findings suggest the existence of a threshold level of expression of *Dlx* for the activation of targets genes.

Human first arch syndromes (FAS) include a wide spectrum of congenital anomalies characterized by defects of CNCC derivatives, and in most cases proximal and not distal jaw structures are affected (Gorlin, 2001). The abnormal traits are associated with different conditions including for example oculo-auriculo-vertebral spectrum (OAVS, OMIM 164210), hemifacial microsomia, mandibulofacial dysostosis, Goldenhar or Franceschetti syndromes. The consequence is a lateral deviation of the mandible accompanied by an anomaly of the dentary occlusion and hearing deficiency. The phenotypes of FAS are strongly suggestive of a defect of CNCCs, and interestingly, targeted inactivation of genes involved in patterning CNCCs often results in proximal defects of the dentary and/or of the middle and external ear (for a recent review see: Gitton *et al.*, 2010). Based on morphological similarities with mouse mutant models, the involvement of Edn1 and putative targets in FAS has been suggested (Kelberman *et al.*, 2001; Masotti *et al.*, 2008; Singer *et al.*, 1994), but not experimentally proven. Our observation on partial allele losses of the Edn1-Dlx pathway might help explain why human FAS affect proximal, rather than distal, derivatives of PA1.

A final general conclusion of our study is that early morphogenetic signals seem to define "large" territories of the craniofacial anlage while subsequent regulations coordinate much more spatio-temporally defined and diversified structures, to specify more "local" shapes of individual elements of the jaw. Distinct time-specific levels of regulation might help to explain the apparent contradiction between data suggesting that CNCCs specification